On the Asymptotic and Numerical Analysis of Exponentially Ill-Conditioned Singularly Perturbed Boundary Value Problems

June-Yub Lee †
Dept. of Mathematics
Courant Institute, New York University
New York, New York 10012

Michael J. Ward *
Dept. of Mathematics
University of British Columbia
Vancouver, Canada V6R 2N4

Abstract

Asymptotic and numerical methods are used to study several classes of singularly perturbed boundary value problems for which the underlying homogeneous operators have exponentially small eigenvalues. Examples considered include the familiar boundary layer resonance problems and some extensions, and certain linearized equations associated with metastable internal layer motion. For the boundary layer resonance problems, a systematic projection method, motivated by the work of De Groen [*SIAM J. Math. Anal.* 11, (1980), pp. 1-22], is used to analytically calculate high order asymptotic solutions. This method justifies and extends some previous results obtained from the variational method of Grasman and Matkowsky [*SIAM J. Appl. Math.* 32, (1977), pp. 588-597]. A numerical approach, based on an integral equation formulation, is used to accurately compute boundary layer resonance solutions and their associated exponentially small eigenvalues. For various examples, the numerical results are shown to compare very favorably with two term asymptotic results. Finally, some Sturm-Liouville operators with exponentially small spectral gap widths are studied. One such problem is applied to analyzing metastable internal layer motion for a certain forced Burgers equation.

† The work of this author was supported by a Packard Foundation fellowship awarded to Leslie Greengard

* Supported by NSERC under grant 5-81541

1. Introduction

For $\epsilon \to 0^+$, we study certain classes of ill-conditioned boundary value problems of the form

$$L_\epsilon u(x) \equiv \epsilon u''(x) + p(x,\epsilon)u'(x) + q(x,\epsilon)u(x) = f(x,\epsilon)\,, \qquad u(a) = \alpha\,, \quad u(b) = \beta\,. \tag{1.1}$$

The problems we consider are those for which the eigenvalue problem $L_\epsilon \phi = \lambda \phi$ with $\phi(a) = \phi(b) = 0$ has an exponentially small eigenvalue λ_0 with $\lambda_0 = O(\epsilon^\nu e^{-\omega \epsilon^{-1}})$ as $\epsilon \to 0$ for some $\omega > 0$.

Examples of operators L_ϵ that have such a spectral property include the exit operator (cf. [22], [23], [6]) and the Hermite operator (cf. [6]). Both of these operators are associated with the well-known boundary layer resonance phenomena that was first discovered in [1] and later studied analytically, from various viewpoints, in [24], [9], [25], [15], [6] and [17] (see also the references therein). More recently, it has been shown that an exponentially small eigenvalue occurs for a certain linearized operator that arises from a nonlinear viscous shock problem exhibiting metastable internal layer motion (cf. [18], [27], [28], [19] and [20]).

For the boundary layer resonance problems, a conventional matched asymptotic expansion approach fails to determine the solutions uniquely. To overcome this deficiency, a variational principle was postulated and used in [9] to calculate leading order asymptotic solutions for these problems. This method was subsequently extended in [34] and [29] to obtain a uniformly valid leading order characterization of the extreme sensitivity of the boundary layer resonance solutions to small changes in the data for (1.1). More recently, a modified variational principle was proposed in [30] to calculate higher order corrections for the solutions.

The relationship between boundary layer resonance phenomena and exponentially small eigenvalues was uncovered and emphasized in [6] (see also [17]). Motivated by this work, our first goal is to formulate and use a systematic projection method to calculate high order asymptotic expansions for the boundary layer resonance solutions and for their associated exponentially small eigenvalues. This method, which explicitly exploits the spectral properties of the homogeneous operator, gives a justification for the postulated variational principle of [9] and its extensions. Moreover, the extreme sensitivity of the boundary layer resonance solutions to small changes in data, and the difficulty in numerically computing such solutions using standard methods, has a very natural interpretation in terms of the exponential ill-conditioning of the underlying homogeneous operator. This spectral approach also provides a unifying link to a related projection approach used recently in [27] and [28] to analyze metastable viscous shock layer motion.

Our second goal is to use the recent numerical method of [21], which is based on an integral equation formulation, to accurately compute boundary layer resonance solutions in response to exponentially small changes in the coefficients of the differential operator. The associated exponentially small eigenvalues are also computed accurately. For a series of examples, numerical results for the boundary layer resonance solutions and the associated small eigenvalues are compared with corresponding asymptotic results. In many cases, these comparisons show that two term asymptotic results are required to obtain a close quantitative agreement with the numerical values. These comparisons then justify the need for the higher order asymptotic theory. To the best of our knowledge, these examples provide the first comprehensive and accurate comparisons between asymptotic and numerical results, at small values of ϵ, for the boundary layer resonance phenomena.

The previous studies of boundary layer resonance have focussed on the homogeneous case $f = 0$ in (1.1). Our third goal is to use the projection method and the numerical method of [21] to examine some inhomogeneous problems. The analysis shows that when f is not orthogonal to the eigenfunction of L_ϵ that corresponds to the exponentially small eigenvalue, the solution of (1.1) is very sensitive to an exponentially small forcing function. These results are then applied to a linearized sensitivity analysis of a model equation of [4] that arises from a diffusive regularization of the shape from shading problem.

As shown in [18], [27], [28], [19] and [20], exponentially small eigenvalues are also associated with metastable viscous shock layer motion. For a particular choice of boundary condition, an asymptotic estimate for the exponentially small eigenvalue was derived in [27]. For Burgers equation, another goal is to derive further eigenvalue estimates relevant to different boundary conditions and to verify these estimates numerically using the method of [21].

We also consider some singularly perturbed Sturm-Liouville operators with exponentially small spectral gap widths. For two exactly solvable such problems, the numerical method of [21] is shown to provide highly accurate results for the small gap widths. Our last focus is to show that a modified version of the symmetric double well potential problem of [12] is directly relevant to analyzing the slow internal layer motion for a class of forced Burgers equation studied previously using finite difference methods in [18]. For this modified double-well problem, an asymptotic formula for the exponentially small spectral gap width is obtained and is verified numerically. The reciprocal of this gap width then determines the metastable time scale for the slow internal layer motion.

The outline of the paper is as follows. In §2 we discuss the favorable properties of the numerical method of [21] for computing both the solutions to exponentially ill-conditioned boundary value problems and their corresponding exponentially small eigenvalues. In §3 and §4 we examine, using analytical and numerical methods, the boundary layer resonance phenomena associated with the exit operator and the Hermite operator, respectively. Inhomogeneous exponentially ill-conditioned problems and an application are considered in §5. In §6 eigenvalue estimates for metastable internal layer motion are derived and verified numerically. Finally, in §7, we consider some nearly degenerate Sturm-Liouville operators, and the results are applied to a a forced Burgers equation.

2. The Numerical Method

There are two inherent obstacles in solving exponentially ill-conditioned problems of the form (1.1) numerically. The first difficulty is that $u(x)$ can be exponentially sensitive to all the data in (1.1); for example, to $f(x)$. More specifically, since the norm of the mapping from f to u is of the order $O(\lambda_0^{-1})$, a perturbation Δf to f may cause rather large changes Δu in u, of the order $O(\lambda_0^{-1}\Delta f)$. Thus one of the necessary conditions for a numerical method to treat these problems is that the numerical error be less than the order of the smallest eigenvalue of the homogeneous operator. However, any numerical method will certainly generate discretization errors by restricting the functional spaces containing p, q, f and u to finite dimensional spaces. Therefore, high order or spectral-type numerical methods, which lead to small residual errors with a moderate number of meshpoints, are preferred for these problems.

The second difficulty is universally encountered when a differential operator L_ϵ is replaced by a discrete operator L_ϵ^h with a parameter h, usually representing mesh size, and evaluated numerically using finite precision arithmetic. Although $||L_\epsilon^h||$ grows without bound when L_ϵ^h approaches L_ϵ

as $h \to 0$, it is still possible to bound the l_2 norm of the numerical operator L_ϵ^h by choosing a fixed size of h. Thus, in spite of the unboundedness of L_ϵ, we can get some digits of accuracy for well-conditioned problems since for some fixed h, the condition number $||L_\epsilon^h||\,||(L_\epsilon^h)^{-1}||$ might be smaller than the reciprocal of the machine precision. However, for ill-conditioned problems where $||(L_\epsilon^h)^{-1}|| \approx 10^{14}$, it is difficult to achieve any accuracy in double precision arithmetic unless $||L_\epsilon^h||$ is of the order of unity.

The requirement of having to simultaneously obtain a small value of $||L_\epsilon^h||$ and a small residual error provides a significant limitation on the use of standard discretizations, such as those based on finite difference or finite element methods, to treat exponentially ill-conditioned problems of the form (1.1). To circumvent this difficulty, we use a high order integral equation scheme for (1.1) whose condition number does not depend on mesh size. Thus, the performance of this numerical method is limited only by the ill-conditioning of the underlying continuous problem.

2.1 Numerical Solutions of Stiff Boundary Value Problems

The solution to (1.1) is decomposed into the sum of two terms; a linear function u_i satisfying the boundary conditions of (1.1) and the solution u_h of (1.1) satisfying homogeneous boundary conditions. In principle, u_h can then be written in terms of the Green's function of L_ϵ. However, since, for arbitrary variable coefficients in L_ϵ, it is not analytically feasible to calculate this Green's function, we instead derive an integral equation for u_h in terms of the Green's function $G_0(x,t)$ of the simpler problem $\phi''(x) - q_0\phi(x) = 0$ with $\phi(a) = \phi(b) = 0$, where q_0 is an arbitrary non-negative constant (see [7] for a discussion of Green's functions).

In terms of $G_0(x,t)$ we define the operator $P : L^2[a,b] \to L^2[a,b]$ by

$$P\eta(x) = \epsilon\eta(x) + p(x)\int_a^b \frac{d}{dx}G_0(x,t)\eta(t)dt + \big(q(x) - q_0\big)\int_a^b G_0(x,t)\eta(t)dt. \tag{2.1}$$

Then, the solution of (1.1) can be written in the form

$$u(x) = u_i(x) + u_h(x) = u_i(x) + \int_a^b G_0(x,t)\sigma(t)\,dt\,, \tag{2.2}$$

where σ satisfies the following Fredholm integral equation of the second kind:

$$P\sigma = f(x) - \big(\epsilon u_i''(x) + p(x)u_i'(x) + q(x)u_i(x)\big)\,. \tag{2.3}$$

From [26], this integral equation is well conditioned in the sense that both P and its inverse P^{-1} are bounded regardless of the mesh size and the order of discretization. In spite of this favorable property, numerical approaches based on integral equation formulations have not been widely used due to the fact that traditional integral equation solvers are computationally more expensive than those for finite difference or finite element methods. Recently, however, some fast methods for integral equations have been developed (cf. [10], [11], and [31]). In particular, a fast adaptive numerical method for stiff two point boundary value problems, which was based on (2.3), was studied and fully described in a paper by one of the present authors (cf. [21]). This method, which is used for all the numerical experiments in this paper, solves (1.1) with an arbitrary order of accuracy at a computational cost proportional to the number of mesh points. For the examples in sections 3 through 6 below, the order of accuracy for the method of [21] was set to 24 and the number of subintervals was set to about 64. These choices were sufficient to resolve the exponentially small changes in the coefficient functions and to obtain full numerical accuracy to within double precision.

2.2 The Numerical Evaluation of Eigenvalues and Eigenfunctions

In sections 3-7, exponentially small eigenvalues for the Sturm-Liouville problem

$$L\phi + \lambda w\phi \equiv (p\phi^{'})^{'} + q\phi + \lambda w\phi = 0\,, \tag{2.4}$$

satisfying certain homogeneous boundary conditions, are computed.

One classical way to compute eigenvalues for (2.4) is to use a shooting method whereby a sequence of initial value problems with unknown parameter λ is solved until λ is adjusted so that both boundary conditions are satisfied. Well-developed software packages that use a shooting approach, such as SLEIGN or the NAG library code D02KDF, are available (see [2], [8], [13] for a further discussion). The difficulty with this method is that it typically requires the numerical determination of a root of a nonlinear shooting function, which may be difficult for ill-conditioned problems.

Another approach for (2.4) is to iteratively approximate eigenvalues and eigenfunctions by solving a sequence of two point boundary value problems. A discussion of subspace methods and their generalizations can be found in the review article [33], while linear algebraic techniques using finite difference and collocation methods are studied in [5], [16].

The approach we use to compute eigenvalues of (2.4) is based on combining an inverse orthogonal iteration method with the integral equation solver of §2.1. Although, the algorithm is fully described in [21], we would like to summarize some important characteristics of the method. Firstly, the convergence of subspace iteration is, in general, linear and the convergence rate depends on the distribution of the eigenvalues. To overcome the slow convergence for the eigenvalue computations, a shifting procedure is performed every iteration to ensure quadratic convergence. This shifting procedure is crucial for the success of the computations in §7 involving nearly degenerate Sturm-Liouville spectra. Roughly 15 iterations are sufficient to obtain double precision accuracy for the examples in this paper. Secondly, the accuracy of the eigenvalues and the eigenfunctions depends on the order of the integral equation method. Therefore, the limit of accuracy is bounded by the conditioning of the underlying continuous problem. The relationship between the smallest eigenvalue and the conditioning is illustrated in Fig. 1 for example 3.1 of §3.

3. The Exit Operator

For $\epsilon \to 0$, we obtain high order asymptotic solutions for

$$\begin{aligned} &L_\epsilon u \equiv \epsilon u^{''} - x^{2m+1}p(x)u^{'} = -g(x)\epsilon^{\nu}e^{-\epsilon^{-1}d}\,u\,, \qquad -a \le x \le b\,, \\ &u(-a) = \alpha\,, \qquad u(b) = \beta\,. \end{aligned} \tag{3.1}$$

Here $a > 0$, $b > 0$, $d > 0$, m is a non-negative integer and $p(x) > 0$ and $g(x)$ are smooth functions. The asymptotic results are verified numerically.

3.1 Spectral Properties

We first study the spectral properties for the eigenvalue problem

$$L_\epsilon \phi = \lambda\, \phi\,, \qquad \phi(-a) = \phi(b) = 0\,. \tag{3.2}$$

For (3.2), the eigenvalues λ_j for $j \geq 0$ are real with $\lambda_j < 0$ for $j \geq 0$ and $\lambda_j \to -\infty$ as $j \to \infty$. The normalized eigenfunctions ϕ_j satisfy $\left(\phi_j, \phi_k\right)_w = \delta_{jk}$, where the inner product is defined by $\left(u, v\right)_w \equiv \int_{-a}^{b} uvw\, dx$. The weight function $w = w(x,\epsilon)$ is defined by

$$w \equiv \exp\left(-\epsilon^{-1} \int_0^x t^{2m+1} p(t)\, dt\right)\,. \tag{3.3}$$

The Rayleigh quotient can be used to show the crude estimate that $\lambda_0 = O\left(\epsilon^q e^{-\epsilon^{-1}\omega}\right)$ for some q and $\omega > 0$. We now calculate λ_0 more precisely.

Let v satisfy $L_\epsilon v = 0$. Then, upon integrating by parts, we derive

$$\lambda_0 \left(v, \phi_0\right)_w = \epsilon w(b) v(b) \phi_0^{'}(b) - \epsilon w(-a) v(-a) \phi_0^{'}(-a)\,. \tag{3.4}$$

Choose $v = 1$ and assume that $\lambda_0 = o(\epsilon^k)$ for any $k > 0$. Then, since $L_\epsilon v = 0$, we have that $\phi_0 \sim M_0$, where M_0 is a normalization constant. However, since this approximate form for ϕ_0 does not satisfy the boundary conditions in (3.2), we must construct boundary layer profiles for ϕ_0 near each endpoint before calculating $\phi_0^{'}(-a)$ and $\phi_0^{'}(b)$.

In the region near $x = -a$ we define $y = \epsilon^{-1}(a + x)$ and $\Phi_L(y) = \phi_0(-a + \epsilon y)$. Then, by substituting $\Phi_L(y) = \Phi_L^0(y) + \epsilon \Phi_L^1(y) + \cdots$ into (3.2) and by using the matching condition $\Phi_L(y) \to M_0$ as $y \to \infty$, we obtain the following boundary layer equations

$$\begin{aligned}
&\Phi_L^{0''} + \xi_a \Phi_L^{0'} = 0\,, \qquad \Phi_L^0(0) = 0\,, \quad \Phi_L^0(y) \to M_0 \;\text{ as }\; y \to \infty\,, \\
&\Phi_L^{1''} + \xi_a \Phi_L^{1'} = \xi_a y \left(\frac{(2m+1)}{a} - \frac{p^{'}(-a)}{p(-a)}\right) \Phi_L^{0'}\,, \qquad \Phi_L^1(0) = 0\,, \quad \Phi_L^1(y) \to 0 \;\text{ as }\; y \to \infty\,.
\end{aligned} \tag{3.5}$$

Here $\xi_a \equiv a^{2m+1} p(-a)$. The solutions to (3.5) are

$$\begin{aligned}
\Phi_L^0(y) &= M_0 \left(1 - e^{-\xi_a y}\right)\,, \\
\Phi_L^1(y) &= M_0 \left(\frac{p^{'}(-a)}{p(-a)} - \frac{(2m+1)}{a}\right) \left(\xi_a \frac{y^2}{2} + y\right) e^{-\xi_a y}\,.
\end{aligned} \tag{3.6}$$

Thus, upon using $\phi_0^{'}(-a) = \epsilon^{-1} \Phi_L^{'}(0)$, we obtain the two term expansion

$$\phi_0^{'}(-a) = M_0 \xi_a \epsilon^{-1} \left[1 + \frac{\epsilon}{\xi_a} \left(\frac{p^{'}(-a)}{p(-a)} - \frac{(2m+1)}{a}\right) + \cdots\right]\,, \qquad \xi_a \equiv a^{2m+1} p(-a)\,. \tag{3.7a}$$

A similar calculation, which we omit, provides the following two term expansion for $\phi_0^{'}(b)$:

$$\phi_0^{'}(b) = -M_0 \xi_b \epsilon^{-1} \left[1 - \frac{\epsilon}{\xi_b} \left(\frac{p^{'}(b)}{p(b)} + \frac{(2m+1)}{b} + \right) + \cdots\right]\,, \qquad \xi_b \equiv b^{2m+1} p(b)\,. \tag{3.7b}$$

By extending the boundary layer analyses to higher order, we can in principle calculate further terms in the expansions of $\phi_0'(-a)$ and $\phi_0'(b)$. For $\epsilon \to 0$, these expansions have the form

$$\begin{aligned} \phi_0'(-a) &= M_0 \xi_a \epsilon^{-1} \gamma_a(\epsilon) , \qquad \gamma_a(\epsilon) \sim 1 + \sum_{j=1}^{\infty} \epsilon^j \phi_{Lj} , \\ \phi_0'(b) &= -M_0 \xi_b \epsilon^{-1} \gamma_b(\epsilon) , \qquad \gamma_b(\epsilon) \sim 1 + \sum_{j=1}^{\infty} \epsilon^j \phi_{Rj} , \end{aligned} \tag{3.8}$$

for some ϕ_{Lj} and ϕ_{Rj} independent of ϵ. The terms ϕ_{L1} and ϕ_{R1} in (3.8) can be read from (3.7).

Next we calculate $\left(v, \phi_0\right)_w$. Since w is concentrated near $x = 0$, this inner product can be calculated using Laplace's method with $v = 1$ and $\phi_0 \sim M_0$ to obtain

$$\left(v, \phi_0\right)_w \sim M_0 \epsilon^{1/(2m+2)} \, \theta_\epsilon , \qquad \theta_\epsilon \sim \sum_{j=0}^{\infty} \epsilon^{j/(m+1)} \theta_j , \tag{3.9a}$$

for some coefficients θ_j independent of ϵ. The first two coefficients are

$$\begin{aligned} \theta_0 &= \frac{r^{1/(2m+2)}}{(m+1)} \Gamma\left(\frac{1}{2m+2}\right) , \\ \theta_1 &= \frac{3 r r^{3/(2m+2)}}{(2m+2)^2} \left(\frac{[p'(0)]^2 (2m+5)}{p(0)(2m+3)^2} - \frac{p''(0)}{(2m+4)} \right) \Gamma\left(\frac{3}{2m+2}\right) , \end{aligned} \tag{3.9b}$$

where $r \equiv 2(m+1)/p(0)$ and $\Gamma(z)$ is the Gamma function. Substituting (3.3), (3.8) and (3.9a) in (3.4), we obtain the following estimate for the exponentially small eigenvalue

$$\lambda_0 \sim -\epsilon^{-1/(2m+2)} \, \theta_\epsilon^{-1} \left[b^{2m+1} p(b) \gamma_b(\epsilon) e^{-\epsilon^{-1} \omega_b} + a^{2m+1} p(-a) \gamma_a(\epsilon) e^{-\epsilon^{-1} \omega_{-a}} \right] . \tag{3.10a}$$

Here $\gamma_a(\epsilon)$ and $\gamma_b(\epsilon)$ are defined by (3.8) while ω_{-a} and ω_b are defined by

$$\omega_{-a} = \int_0^{-a} t^{2m+1} p(t) \, dt , \qquad \omega_b = \int_0^b t^{2m+1} p(t) \, dt . \tag{3.10b}$$

For the case $m = 0$ and upon replacing θ_ϵ, γ_a and γ_b in (3.10a) by their leading behaviors $\theta_\epsilon \sim \theta_0$, $\gamma_a \sim 1$ and $\gamma_b \sim 1$, the resulting leading order formula for λ_0 was proven in [6]. Similar leading order eigenvalue estimates for some related equations were derived in [22] and [23].

We now consider two special cases of (3.10a). Assume that $a = b$, $m = 0$ and that $p(x)$ is an even function. Then, using (3.7), (3.9b) and (3.10a), we obtain the two term expansion

$$\lambda_0 \sim -\left(\frac{2p(0)}{\pi\epsilon}\right)^{1/2} b p(b) \left[1 + \epsilon \left(\frac{3p''(0)}{8[p(0)]^2} - \frac{1}{bp(b)} \left(\frac{1}{b} + \frac{p'(b)}{p(b)}\right) \right) \right] \exp\left(-\epsilon^{-1} \int_0^b t p(t) \, dt \right) . \tag{3.11a}$$

When $p(x)$ is even, $a = b$ and $m = 1$, we have the two term expansion

$$\lambda_0 \sim -\left(\frac{p(0)}{4\epsilon}\right)^{1/4} \frac{4b^3 p(b)}{\Gamma(1/4)} \left[1 + \epsilon^{1/2} \frac{p''(0)}{16} \left(\frac{4}{p(0)}\right)^{3/2} \frac{\Gamma(3/4)}{\Gamma(1/4)} \right] \exp\left(-\epsilon^{-1} \int_0^b t^3 p(t) \, dt \right) . \tag{3.11b}$$

We now give illustrate (3.11) for some specific forms of $p(x)$. The motivation for considering these forms of $p(x)$ is given in §5.2. Let $p(x) = 2\pi x^{-1}\sin(\pi x/2)$, $b = 1$ and $m = 0$. Then (3.11a) becomes

$$\lambda_0 \sim -(2\pi)^{3/2}\epsilon^{-1/2}\left(1 - \frac{\epsilon}{32}\right) e^{-4\epsilon^{-1}} . \tag{3.12a}$$

Now let $p(x) = 2\pi(1+\mu x^2)^{-1}$, $\mu \geq 0$, $b = 1$ and $m = 1$. Then (3.11b) becomes

$$\lambda_0 \sim -\left(\frac{\pi}{2\epsilon}\right)^{1/4} \frac{8\pi}{(1+\mu)}[\Gamma(1/4)]^{-1}\left(1 - \frac{\epsilon^{1/2}\mu}{2}\left(\frac{2}{\pi}\right)^{1/2}\frac{\Gamma(3/4)}{\Gamma(1/4)}\right) e^{-\epsilon^{-1}\omega_1} , \tag{3.12b}$$

where $\omega_1 = \pi\mu^{-1}[1 - \mu^{-1}\log(1+\mu)]$. In the special case when $\mu = 0$ we can calculate an additional term in (3.12b). When $\mu = 0$ we have $\theta_\epsilon = \theta_0 + o(\epsilon^k)$ for any $k > 0$. Thus, in this case, (3.8) and (3.10) yield

$$\lambda_0 \sim -\left(\frac{\pi}{2\epsilon}\right)^{1/4} \frac{8\pi}{\Gamma(1/4)}\left(1 - \frac{3\epsilon}{2\pi}\right) e^{-\epsilon^{-1}\pi/2} . \tag{3.12c}$$

To compare with (3.12), we use the eigenvalue solver of [21], summarized in §2, to compute λ_0 directly from (3.2). In Tables 1a, 1b and 1c we display the results for λ_0 corresponding to (3.12a), (3.12b) with $\mu = 1$, and (3.12c), respectively. In each of these tables, the second column gives the numerical result for λ_0 while the third column gives the two term expansion for λ_0. In the fourth column we also display the results for λ_0 that are obtained by truncating the pre-exponential factors in (3.12) to one term. Several trends can be observed from these comparisons. We first note that a two term expansion for the pre-exponential factor of λ_0 is needed to obtain close quantitative agreement with the numerical results. In certain cases, the agreement between the two term result and the numerical result is close even at rather large values of ϵ (see the first few rows of Table 1a and Table 1c). From Table 1b we note that when the pre-exponential factor for λ_0 has an expansion in powers of $\epsilon^{1/2}$, the two term asymptotic result gives only a moderately good determination of λ_0. Finally, we note that the numerical method for calculating λ_0 becomes inaccurate when $\lambda_0 \approx 10^{-15}$ (see the last row in each of these tables).

3.2 The Projection Method

We now solve (3.1) asymptotically for $\epsilon \to 0$. Since $d > 0$, the composite matched asymptotic expansion for the solution to (3.1) is given in terms of an undetermined constant C_0 by

$$\tilde{u}^\epsilon(x) = C_0 + (\alpha - C_0)\, e^{-\xi_a \epsilon^{-1}(a+x)} + (\beta - C_0)\, e^{-\xi_b \epsilon^{-1}(b-x)} . \tag{3.13}$$

Here $\xi_a \equiv a^{2m+1}p(-a)$ and $\xi_b = b^{2m+1}p(b)$. We now describe the projection method, motivated by the work of [6], to determine C_0. Defining $v = u - \tilde{u}^\epsilon$, and assuming that $v \ll \tilde{u}^\epsilon$, we find from (3.1) that v satisfies the approximate equation

$$L_\epsilon v = -L_\epsilon \tilde{u}^\epsilon - g(x)\epsilon^\nu e^{-\epsilon^{-1}d}\tilde{u}^\epsilon , \tag{3.14a}$$

$$v(-a) = \alpha - \tilde{u}^\epsilon(-a) , \qquad v(b) = \beta - \tilde{u}^\epsilon(b) . \tag{3.14b}$$

We then expand v in terms of the eigenfunctions ϕ_j of (3.2) to obtain

$$v = \sum_{j=0}^{\infty} \frac{A_j}{\lambda_j}\phi_j , \qquad A_j = \epsilon w v \phi_j^{'} \Big|_{-a}^{b} - \left(\phi_j, L_\epsilon \tilde{u}^\epsilon\right)_w - \epsilon^\nu e^{-\epsilon^{-1}d}\left(\phi_j, g\tilde{u}^\epsilon\right)_w . \tag{3.15}$$

Since $\lambda_0 \to 0$ as $\epsilon \to 0$, a necessary condition for (3.14) to have a solution in this limit is that $A_0 \to 0$ as $\epsilon \to 0$. The condition $A_0 = 0$, which eliminates the largest component in v, provides the following equation for C_0:

$$-\epsilon^{\nu} e^{-\epsilon^{-1} d} \left(\phi_0, g\tilde{u}^{\epsilon}\right)_w = \left(\phi_0, L_{\epsilon}\tilde{u}^{\epsilon}\right)_w - \epsilon w v \phi_0' \Big|_{-a}^{b} . \tag{3.16}$$

For $\epsilon \to 0$, we now evaluate the terms in (3.16). Using Laplace's method we can calculate the asymptotic expansion of $\left(\phi_0, g\tilde{u}^{\epsilon}\right)_w$ in terms of the behavior of w, ϕ_0 and $\tilde{u}^{\epsilon}$ near $x = 0$. This method yields

$$\left(\phi_0, g\tilde{u}^{\epsilon}\right)_w \sim C_0 \left(\phi_0, g\right)_w \sim M_0 C_0 \epsilon^{1/(2m+2)} g_{\epsilon} , \qquad g_{\epsilon} \sim \sum_{j=0}^{\infty} \epsilon^{j/(m+1)} B_j , \tag{3.17a}$$

for some coefficients B_j independent of ϵ. The first two coefficients are

$$\begin{aligned} B_0 &= \frac{r^{1/(2m+2)}}{(m+1)} g(0) \Gamma\left(\frac{1}{2m+2}\right) , \\ B_1 &= \frac{3r^{3/(2m+2)}}{(2m+2)^2} \left[\frac{(2m+2)}{3} g''(0) - r\left(\frac{2p'(0)g'(0)}{2m+3} + \frac{p''(0)g(0)}{2m+4} \right) \right] \Gamma\left(\frac{3}{2m+2}\right) \\ &\quad + \frac{3r^2 r^{3/(2m+2)}}{(2m+2)^3} \frac{(2m+5)}{(2m+3)^2} [p'(0)]^2 g(0) \Gamma\left(\frac{3}{2m+2}\right) , \end{aligned} \tag{3.17b}$$

where $r \equiv 2(m+1)/p(0)$. Next, to evaluate $\left(\phi_0, L_{\epsilon}\tilde{u}^{\epsilon}\right)_w$ we first integrate by parts to derive the identity

$$\left(\phi_0, L_{\epsilon}\tilde{u}^{\epsilon}\right)_w = -\epsilon \left(\tilde{u}_L^{\epsilon} + \tilde{u}_R^{\epsilon}\right) \phi_0' w \Big|_{-a}^{b} + \lambda_0 \left(\phi_0, \tilde{u}_L^{\epsilon}\right)_w + \lambda_0 \left(\phi_0, \tilde{u}_R^{\epsilon}\right)_w , \tag{3.18a}$$

where $\tilde{u}_L^{\epsilon} = (\alpha - C_0) e^{-\xi_a \epsilon^{-1}(a+x)}$ and $\tilde{u}_R^{\epsilon} = (\beta - C_0) e^{-\xi_b \epsilon^{-1}(b-x)}$. Since λ_0 is exponentially small, (3.18a) reduces to

$$\left(\phi_0, L_{\epsilon}\tilde{u}^{\epsilon}\right)_w \sim \epsilon w(-a)[\alpha - C_0]\phi_0'(-a) - \epsilon w(b)[\beta - C_0]\phi_0'(b) . \tag{3.18b}$$

From (3.14b) and (3.13) we note that $v(-a)$ and $v(b)$ are both exponentially small. Thus, the second term on the right side of (3.16) can be neglected in comparison with $\left(\phi_0, L_{\epsilon}\tilde{u}^{\epsilon}\right)_w$. Next, we substitute (3.17a) and (3.18b) in (3.16) to obtain the following equation for C_0

$$-\epsilon^{\nu + 1/(2m+2)} C_0 g_{\epsilon} e^{-\epsilon^{-1} d} \sim b^{2m+1} p(b) \left(\beta - C_0\right) \gamma_b e^{-\epsilon^{-1}\omega_b} + a^{2m+1} p(-a) \left(\alpha - C_0\right) \gamma_a e^{-\epsilon^{-1}\omega_{-a}} . \tag{3.19}$$

Finally, $\tilde{u}^{\epsilon}$ is given in terms of C_0 by (3.13). We now consider some special cases of (3.19).
Case 1: Assume that $d > \max(\omega_{-a}, \omega_b)$. Then, from (3.19), C_0 satisfies

$$C_0 \sim \left(\frac{\alpha a^{2m+1} p(-a)\gamma_a}{b^{2m+1} p(b)\gamma_b} e^{\epsilon^{-1}(\omega_b - \omega_{-a})} + \beta \right) \left(\frac{a^{2m+1} p(-a)\gamma_a}{b^{2m+1} p(b)\gamma_b} e^{\epsilon^{-1}(\omega_b - \omega_{-a})} + 1 \right)^{-1} . \tag{3.20}$$

When $\omega_b > \omega_{-a}$, then $C_0 \sim \alpha$ and there is no boundary layer at $x = -a$. When $\omega_{-a} < \omega_b$, then $C_0 \sim \beta$ and there is no boundary layer at $x = b$. For $|\omega_b - \omega_{-a}| = O(\epsilon)$, (3.20) provides a uniform transition between these two limiting behaviors for C_0. For $m=0$, a leading order calculation for this transition behavior, in which $\gamma_a \sim 1$ and $\gamma_b \sim 1$, was derived in [29] using the variational method of [9].

Case 2: Assume that $|d-\omega_b| = O(\epsilon)$, $\omega_{-a} > \omega_b$ and $\nu = -1/(2m+2)$. In this case boundary layers exist at both endpoints and

$$C_0 \sim \beta \left(1 - \frac{g_\epsilon b^{-2m-1}}{p(b)\gamma_b} e^{\epsilon^{-1}(\omega_b - d)}\right)^{-1} . \tag{3.21}$$

Setting $m=0$ and replacing g_ϵ and γ_b by their leading terms $g_\epsilon \sim \left[2\pi/p(0)\right]^{1/2} g(0)$ and $\gamma_b \sim 1$ as $\epsilon \to 0$, we find that (3.21) agrees with the result in [34].

Case 3: Assume that $|d-\omega_b| = O(\epsilon)$, $\omega_{-a} = \omega_b$ and $\nu = -1/(2m+2)$. Then, boundary layers exist at both endpoints and

$$C_0 \sim \left(\beta b^{2m+1} p(b)\gamma_b + \alpha a^{2m+1} p(-a)\gamma_a\right) \left(b^{2m+1} p(b)\gamma_b + a^{2m+1} p(-a)\gamma_a - g_\epsilon \, e^{\epsilon^{-1}(\omega_b - d)}\right)^{-1} . \tag{3.22}$$

If, in addition, $p(x)$ is an even function, then $a=b$, $\gamma_a = \gamma_b$ and so

$$C_0 \sim (\beta + \alpha) \left(2 - \frac{g_\epsilon b^{-2m-1}}{p(b)\gamma_b} e^{\epsilon^{-1}(\omega_b - d)}\right)^{-1} . \tag{3.23}$$

3.3 Examples and Computations

We now give some examples of the theory. The asymptotic results are confirmed by direct numerical computations on (3.1).

Example 3.1: For $b > 0$ and $\mu \geq 0$, consider

$$\begin{aligned} &\epsilon u'' - \frac{2\pi x^3}{(1+\mu x^2)} u' = -s\epsilon^{-1/4}(1+x^2) e^{-\epsilon^{-1} d} u \,, \qquad -1 \leq x \leq b \,, \\ &u(-1) = 1 \,, \qquad u(b) = 2 \,. \end{aligned} \tag{3.24}$$

Thus $p(x) = 2\pi(1+\mu x^2)^{-1}$, $a=1$, $m=1$ and $\nu = -1/4$. We first let $s=0$ in (3.24). Then, from (3.8), (3.10b) and (3.20) we obtain that

$$C_0 \sim \frac{\rho_\epsilon e^{\epsilon^{-1}(\omega_b - \omega_{-1})} + 2}{\rho_\epsilon e^{\epsilon^{-1}(\omega_b - \omega_{-1})} + 1} \,, \qquad \rho_\epsilon \sim \frac{(1+\mu b^2)}{b^3(1+\mu)} \left[1 - \frac{\epsilon}{2\pi}\left(\mu + 3 - \frac{(3+\mu b^2)}{b^4}\right)\right] , \tag{3.25}$$

where $\omega_b = \pi\mu^{-1}[b^2 - \mu^{-1}\log(1+\mu b^2)]$. To compare with (3.25), solutions to (3.24) were computed using the method of [21]. For the case $b=1$ and $\mu=0$, in Table 2a we compare the numerical value of C_0, defined by $C_0 = u(0)$, with the *exact* value $C_0 = 1.5$. Therefore, the third column in this table shows the loss of precision in the computations as ϵ is decreased. From (3.12c), we note that $\lambda_0 \approx -3.4 \times 10^{-15}$ when $\epsilon = 1/23$ and $\lambda_0 \approx -1.5 \times 10^{-16}$ when $\epsilon = 1/25$. Even in the presence of such an extreme ill-conditioning, the numerical method is able to accurately capture the first few significant digits of C_0. For $\mu = 0$ and for $\mu = 1$, in Fig. 1 we show the loss of accuracy of the numerically computed value of C_0 as $\epsilon \to 0$. The eigenvalue λ_0 is also plotted in this figure. For the case $\mu = 1$ with $\epsilon = 1/36$, in Table 2b we show the very close agreement between the numerical value of C_0 and the asymptotic value (3.25) as b is varied in an $O(\epsilon)$ neighborhood of $b = 1$.

Now let $s = 1$ in (3.24). Then, from (3.10b), (3.17), (3.21) and (3.23) we have that

$$C_0 \sim 2\left[1 - \frac{(1+\mu b^2)}{2\pi b^3 \gamma_b}\left(B_0 + \epsilon^{1/2} B_1\right) e^{\epsilon^{-1}(\omega_b - d)}\right]^{-1}, \qquad b < 1\,, \ |d - \omega_b| = O(\epsilon)\,, \quad (3.26a)$$

$$C_0 \sim 3\left[2 - \frac{(1+\mu)}{2\pi \gamma_1}\left(B_0 + \epsilon^{1/2} B_1\right) e^{\epsilon^{-1}(\omega_1 - d)}\right]^{-1}, \qquad b = 1\,, \ |d - \omega_1| = O(\epsilon)\,. \quad (3.26b)$$

Here B_0, B_1 and γ_b are given by

$$B_0 = \frac{1}{2}\left(\frac{2}{\pi}\right)^{1/4} \Gamma(1/4)\,, \qquad B_1 = \frac{1}{4}\left(\frac{2}{\pi}\right)^{3/4} (2+\mu)\,\Gamma(3/4)\,,$$
$$\gamma_b \sim 1 - \frac{\epsilon(1+\mu b^2)}{2\pi b^4}\left(\frac{3+\mu b^2}{1+\mu b^2}\right)\,. \qquad (3.27)$$

For the case $s = 1$, $b = 1$, $d = \pi/2$ and $\mu = 0$, in Table 2c we compare the numerical value of C_0 at various ϵ with the asymptotic result (3.26b). Then, setting $\epsilon = 1/20$, in Table 2d we compare C_0 values as d is varied in a narrow range near $d = \omega_1 = \pi/2$. In Fig. 2 we plot C_0 versus $z = \epsilon^{-1}(d - \pi/2)$ and we also show the numerical solutions to (3.24) for some selected values of z. Now setting $b = 3/4$, $\mu = 0$ and $\epsilon = 1/36$, in Table 2e we compare the numerical C_0 with the asymptotic result (3.26a) as d is varied near $d = \omega_b$. From Tables 2b-e we observe that (3.26a, b) provides a very close determination of the corresponding numerical result. We remark, however, that the agreement between the asymptotic and numerical values of C_0 is not nearly as close if only the leading term $\gamma_b \sim 1$ is used in (3.26). As seen from Table 2d, we emphasize that the numerical method of [21] gives an accurate result for C_0, even when the numerical value of the perturbing term in (3.24) is roughly $e^{-\epsilon^{-1}d} \approx e^{-\epsilon^{-1}\pi/2} = 2.3 \times 10^{-14}$.

We now interpret the apparent singularity in the plot of $C_0 = C_0(d)$ shown in Fig. 2. This singular-type behavior is rather analogous to a similar behavior that was found in [35] to occur for the related problem $L_\epsilon u = \eta \lambda_0 u$ on $-1 < x < 1$. Here η is a constant, L_ϵ is given in (3.1), $p(x)$ is even, λ_0 is the exponentially small eigenvalue of (3.2) and $u(-1) = \alpha$, $u(1) = \beta$. Clearly this related problem has no solution if $\eta = 1$. The outer solution for this problem is easily shown to be $u \sim C_0 = (1-\eta)^{-1}(\beta + \alpha)/2$. Thus as $\eta \to 1$, C_0 becomes unbounded and the plot of C_0 versus η is qualitatively rather similar to that shown in Fig. 2. This analogy is not entirely satisfactory in that we believe that the true curve $C_0 = C_0(d)$ for example 3.1 is in fact bounded on closed intervals containing $d = \pi/2$ for each fixed ϵ. However, as $\epsilon \to 0$, we expect that $C_0 = C_0(d)$ can become very large at a certain value of d.

Example 3.2: For $b > 0$, consider

$$\epsilon u'' - x\left(x^2 - \frac{7}{4}x + 1\right)u' = -\epsilon^{-1/2}(1+x^2)e^{-\epsilon^{-1}d}u\,, \qquad -1 \le x \le b\,,$$
$$u(-1) = 1\,, \qquad u(b) = 2\,. \qquad (3.28)$$

Thus $m = 0$, $\nu = -1/2$ and $p(x)$ is not even. From (3.10b) we find that $\omega_{-1} > \omega_b$ when $b < 2$ and that $\omega_{-1} = \omega_2 = 4/3$. First suppose that $b = 2$ and $|d - 4/3| = O(\epsilon)$. Then, from (3.8), (3.17) and

(3.22) we calculate that

$$C_0 \sim (39 - 24\epsilon)\left[27 - 16\epsilon - 4(2\pi)^{1/2}\left(1 + \frac{269\epsilon}{96}\right)e^{-\epsilon^{-1}(d-4/3)}\right]^{-1}, \quad b = 2\,, \ |d - 4/3| = O(\epsilon)\,. \tag{3.29}$$

Thus, when $d > 4/3$, $C_0 \sim 13/9 - 8\epsilon/243$. Fixing $d = 4/3$, in Table 3a we compare, at decreasing values of ϵ, the asymptotic result (3.29) with the numerical result for C_0 computed from (3.28). The numerical value of C_0 is again defined by $C_0 = u(0)$.

Next, when $b < 2$ and $|d - \omega_b| = O(\epsilon)$, (3.8), (3.17) and (3.21) provide

$$C_0 \sim 2\rho_\epsilon\left[\rho_\epsilon - (2\pi)^{1/2}\left(1 + \frac{269\epsilon}{96}\right)e^{-\epsilon^{-1}(d-\omega_b)}\right]^{-1}, \quad b < 2\,, \ |d - \omega_b| = O(\epsilon)\,. \tag{3.30}$$

Here ρ_ϵ and ω_b are given by

$$\rho_\epsilon \sim b\left(b^2 - \frac{7}{4}b + 1\right) - \frac{\epsilon}{b}\left(b^2 - \frac{7}{4}b + 1\right)^{-1}\left(3b^2 - \frac{7}{2}b + 1\right), \qquad \omega_b = \frac{b^2}{4}\left(b^2 - \frac{7}{3}b + 2\right). \tag{3.31}$$

Fixing $b = 1$ and $\epsilon = 1/60$, in Table 3b we compare the asymptotic and numerical values of C_0 as d is varied in a narrow range near $d = \omega_b$. From Tables 3a, 3b we note that the agreement between the asymptotic and numerical results for C_0 is moderately good but is not as close as for the previous example.

Example 3.3: Bohé [3] showed that the viscous shock problem

$$\epsilon x'' = -x(x')^2\,, \quad \alpha \le u \le \beta\,, \quad x(\alpha) = -1\,, \quad x(\beta) = b > 0\,, \tag{3.32}$$

for $x = x(u)$ can be mapped, using the inverse mapping $u = u(x)$, to the following example of (3.1):

$$\epsilon u'' - xu' = 0\,, \quad -1 \le x \le b\,, \quad u(-1) = \alpha\,, \quad u(b) = \beta\,. \tag{3.33}$$

The qualitative behavior of the shock layer location for (3.32) in response to small changes in b for b near 1 was discussed in [3]. To quantify this behavior, we note that the outer solution $u \sim C_0$ for (3.33), where

$$C_0 \sim \frac{\alpha\rho_\epsilon\, e^{\epsilon^{-1}(b^2-1)/2} + \beta}{\rho_\epsilon\, e^{\epsilon^{-1}(b^2-1)/2} + 1}\,, \qquad \rho_\epsilon \sim b^{-1}[1 - \epsilon(1 - b^{-2})]^2\,, \tag{3.34}$$

determines the shock layer location for (3.32). Thus, as b increases (decreases) past one, the shock layer tends to the left (right) endpoint according to (3.34). For several values of $z = \epsilon^{-1}(b-1)$ and for $\alpha = -1$, $\beta = 1$ and $\epsilon = 1/60$, in Fig. 3 we plot the shock layer solution to (3.32), which is computed numerically using (3.33).

4. The Hermite Operator

We now consider the boundary value problem

$$\begin{gathered} L_\epsilon u \equiv \epsilon u'' - xu' + Nu = -g(x)\epsilon^\nu e^{-\epsilon^{-1}d}u\,, \qquad -a \le x \le b\,, \\ u(-a) = \alpha\,, \qquad u(b) = \beta\,. \end{gathered} \tag{4.1}$$

Here $a > 0$, $b > 0$, $d > 0$, N is a nonnegative integer, $g(x)$ is a smooth function and $\epsilon \ll 1$.

4.1 Spectral Properties

As in §3.1, we must first analyze the spectral properties associated with the eigenvalue problem (3.2) where L_ϵ is now defined in (4.1). For this problem, the eigenvalues λ_j for $j \geq 0$ are real with $\lambda_j \to N - j$ as $\epsilon \to 0$. The corresponding normalized eigenfunctions ϕ_j satisfy $\left(\phi_j, \phi_k\right)_w = \delta_{jk}$, where the weight function is given by $w = w(x,\epsilon) = e^{-\epsilon^{-1}x^2/2}$. The eigenvalue λ_N is exponentially small as $\epsilon \to 0$ and we now estimate it precisely.

Let v satisfy $L_\epsilon v = 0$. Then, upon integrating by parts, we derive

$$\lambda_N \left(v, \phi_N\right)_w = \epsilon w(b) v(b) \phi_N^{'}(b) - \epsilon w(-a) v(-a) \phi_N^{'}(-a) . \tag{4.2}$$

Choose $v = \mathrm{He}_N\left(\epsilon^{-1/2}x\right)$, where $\mathrm{He}_N(z)$ is the Hermite poynomial of degree N, and assume that $\lambda_N = o(\epsilon^k)$ for any $k > 0$. Then, since $L_\epsilon v = 0$, we have that $\phi_N \sim M_N \mathrm{He}_N\left(\epsilon^{-1/2}x\right)$ away from $O(\epsilon)$ regions near the endpoints at $x = -a$ and $x = b$. Here M_N is a normalization constant. However, since this approximate form for ϕ_N does not satisfy the homogeneous boundary conditions in (3.2), we cannot use it to calculate $\phi_N^{'}(-a)$ and $\phi_N^{'}(b)$ in (4.2). Instead, these quantities are evaluated after constructing boundary layer profiles for ϕ_N near each endpoint.

In the region near $x = -a$ define $y = \epsilon^{-1}(a + x)$ and $\Phi_L(y) = \phi_N[-a + \epsilon y]$. Then, by expanding

$$\Phi_L(y) = \epsilon^{-N/2}\Phi_L^0(y) + \epsilon^{1-N/2}\Phi_L^1(y) + \cdots , \tag{4.3}$$

we obtain, after equating powers of ϵ in $L_\epsilon \phi_N = 0$, the following boundary layer equations:

$$\begin{aligned} &\Phi_L^{0''} + a\Phi_L^{0'} = 0 , \quad \Phi_L^0(0) = 0 , \qquad y > 0 , \\ &\Phi_L^{1''} + a\Phi_L^{1'} = y\Phi_L^{0'} - N\Phi_L^0 , \quad \Phi_L^1(0) = 0 , \qquad y > 0 . \end{aligned} \tag{4.4}$$

The solutions to (4.4) will match as $y \to \infty$ to the outer solution $\phi_N = M_N \mathrm{He}_N\left(\epsilon^{-1/2}x\right)$ provided that

$$\Phi_L^0(y) \sim M_N(-a)^N , \quad \text{as} \quad y \to \infty ; \quad \Phi_L^1(y) \sim M_N(-a)^{N-2}[h_N - aNy] , \quad \text{as} \quad y \to \infty . \tag{4.5}$$

In (4.5), h_N is defined by

$$h_N = \lim_{z\to\infty} z^{2-N}\left[\mathrm{He}_N(z) - z^N\right] , \qquad \text{so that} \qquad h_N = -N(N-1)/2 . \tag{4.6}$$

From (4.4) and (4.5) we calculate that

$$\begin{aligned} &\Phi_L^0(y) = M_N(-a)^N\left(1 - e^{-ay}\right) , \\ &\Phi_L^1(y) = M_N(-a)^{N-2}\left[h_N - aNy - \left(\frac{1}{2}a^2y^2 + a(1+N)y + h_N\right)e^{-ay}\right] . \end{aligned} \tag{4.7}$$

Finally, using (4.3), (4.7) and $\phi_N^{'}(-a) = \epsilon^{-1}\Phi_L^{'}(0)$ we obtain the two term expansion

$$\phi_N^{'}(-a) = -M_N(-a)^{N+1}\epsilon^{-1-N/2}\left[1 - (2N + 1 - h_N)\frac{\epsilon}{a^2} + \cdots\right] . \tag{4.8a}$$

A similar calculation provides the following two term expansion for $\phi_N^{'}(b)$:

$$\phi_N^{'}(b) = -M_N b^{N+1} \epsilon^{-1-N/2} \left[1 - (2N+1-h_N)\frac{\epsilon}{b^2} + \cdots \right] . \tag{4.8b}$$

Further terms in the expansions of $\phi_N^{'}(-a)$ and $\phi_N^{'}(b)$ can, in principle, be obtained by calculating higher order boundary layer corrections for ϕ_N. These expansions have the form

$$\phi_N^{'}(-a) \sim -M_N(-a)^{N+1}\epsilon^{-1-N/2} \left(1+\sum_{j=1}^{\infty} \epsilon^j \phi_{Lj}\right) , \qquad \phi_N^{'}(b) \sim -M_N b^{N+1}\epsilon^{-1-N/2} \left(1+\sum_{j=1}^{\infty} \epsilon^j \phi_{Rj}\right) , \tag{4.9}$$

for some coefficients ϕ_{Lj} and ϕ_{Rj} independent of ϵ. From (4.8) we have $\phi_{L1} = -a^{-2}(2N+1-h_N)$ and $\phi_{R1} = -b^{-2}(2N+1-h_N)$.

Next, for $\epsilon \to 0$ we estimate the left side of (4.2) to obtain

$$\left(v, \phi_N\right)_w \sim M_N \epsilon^{1/2} \int_{-\infty}^{\infty} e^{-z^2/2} [\mathrm{He}_N(z)]^2 \, dz = M_N \epsilon^{1/2} \left(2\pi\right)^{1/2} N! \, . \tag{4.10}$$

Finally, substituting (4.9), (4.10), $v = \mathrm{He}_N(\epsilon^{-1/2}x)$ and $w = e^{-\epsilon^{-1}x^2/2}$ in (4.2), we obtain the following estimate for the exponentially small eigenvalue λ_N:

$$\lambda_N \sim -\frac{\epsilon^{-N-1/2}}{\left(2\pi\right)^{1/2} N!} \left[b^{2N+1}\gamma_b(\epsilon) e^{-\epsilon^{-1}b^2/2} + a^{2N+1}\gamma_a(\epsilon) e^{-\epsilon^{-1}a^2/2} \right] . \tag{4.11}$$

In (4.11), $\gamma_a(\epsilon)$ and $\gamma_b(\epsilon)$ are defined by

$$\gamma_a(\epsilon) = \frac{\mathrm{He}_N(-\epsilon^{-1/2}a)}{\epsilon^{-N/2}(-a)^N} \left(1 + \sum_{j=1}^{\infty} \phi_{Lj}\epsilon^j \right) , \qquad \gamma_b(\epsilon) = \frac{\mathrm{He}_N(\epsilon^{-1/2}b)}{\epsilon^{-N/2} b^N} \left(1 + \sum_{j=1}^{\infty} \phi_{Rj}\epsilon^j \right) . \tag{4.12a}$$

Clearly γ_a and γ_b can be written as series in powers of ϵ. In particular, from (4.6), (4.8) and (4.9) we obtain the explicit two term expansions

$$\gamma_a(\epsilon) \sim 1 - \left(N^2 + N + 1\right) \frac{\epsilon}{a^2} , \qquad \gamma_b(\epsilon) \sim 1 - \left(N^2 + N + 1\right) \frac{\epsilon}{b^2} . \tag{4.12b}$$

Thus, in the special case when $a = b$, a two term expansion for λ_N, obtained from (4.11), is

$$\lambda_N \sim -\frac{2\,\epsilon^{-N-1/2}}{\left(2\pi\right)^{1/2} N!} b^{2N+1} \left[1 - (N^2+N+1)\frac{\epsilon}{b^2} \right] e^{-\epsilon^{-1}b^2/2} . \tag{4.13}$$

The leading order result for λ_N, obtained by replacing the pre-exponential factor in (4.13) by its leading order behavior, was proven in [6].

The eigenvalue solver of [21] is then used to compute λ_N numerically when $a = b = 1$. In Tables 4a and 4b we compare the numerical results for λ_N against the corresponding asymptotic result (4.13) (with $b = 1$) for the case $N = 1$ and $N = 2$, respectively. In these tables we also give the asymptotic result for λ_N that occurs from truncating the pre-exponential factor in (4.13) to one term. From these tables we note that the two term result provides a significantly better determination of λ_N than does the one term result. As seen from the last row of Table 4a, we note that the numerical result for λ_N becomes inaccurate only when $\lambda_0 \approx 10^{-14}$.

4.2 The Projection Method

We now solve (4.1) in the limit $\epsilon \to 0$. The composite matched asymptotic expansion for the solution to (4.1) is given in terms of an undetermined constant C_0 by

$$\tilde{u}^\epsilon(x) = \left[\alpha - C_0(-a)^N\right] e^{-a\epsilon^{-1}(a+x)} + \left[\beta - C_0 b^N\right] e^{-b\epsilon^{-1}(b-x)} + C_0\epsilon^{N/2}\mathrm{He}_N\left(\epsilon^{-1/2}x\right) . \quad (4.14)$$

Defining v by $v = u - \tilde{u}^\epsilon$, and assuming that $v \ll \tilde{u}^\epsilon$, we obtain from (4.1) that v satisfies the approximate equation

$$L_\epsilon v = -L_\epsilon \tilde{u}^\epsilon - g(x)\epsilon^\nu e^{-\epsilon^{-1}d}\tilde{u}^\epsilon , \quad (4.15a)$$

$$v(-a) \sim C_0\left[(-a)^N - \epsilon^{N/2}\mathrm{He}_N(-\epsilon^{-1/2}a)\right] , \quad v(b) \sim C_0\left[b^N - \epsilon^{N/2}\mathrm{He}_N(\epsilon^{-1/2}b)\right] . \quad (4.15b)$$

Next, we expand v in terms of the eigenfunctions of $L_\epsilon\phi = \lambda\phi$ to obtain the form (3.15). Since $\lambda_N \to 0$ as $\epsilon \to 0$, a necessary condition for the solvability of (4.15) is that $A_N \to 0$ as $\epsilon \to 0$, where A_N is given in (3.15). Setting $A_N = 0$ we find that C_0 satisfies

$$-\epsilon^\nu e^{-\epsilon^{-1}d}\left(\phi_N, g\tilde{u}^\epsilon\right)_w = \left(\phi_N, L_\epsilon\tilde{u}^\epsilon\right)_w - \epsilon w v \phi_N' \Big|_{-a}^{b} . \quad (4.16)$$

For $\epsilon \to 0$, we now evaluate the terms in (4.16). With $\phi_N \sim M_N \mathrm{He}_N(\epsilon^{-1/2}x)$, the inner product $\left(\phi_N, g\tilde{u}^\epsilon\right)_w$ is evaluated by Laplace's method to obtain

$$\left(\phi_N, g\tilde{u}^\epsilon\right)_w \sim M_N C_0 \epsilon^{(N+1)/2}(2\pi)^{1/2} g_\epsilon\, N! , \quad \text{where} \quad g_\epsilon \sim g(0) + \sum_{j=1}^{\infty} \epsilon^j \theta_j g^{(2j)}(0) . \quad (4.17a)$$

Here θ_j is defined by

$$\theta_j = \frac{(2\pi)^{-1/2}}{N!(2j)!}\int_{-\infty}^{\infty} z^{2j}[\mathrm{He}_N(z)]^2 e^{-z^2/2}\, dz , \qquad j = 1, 2, \ldots \quad (4.17b)$$

In particular, $\theta_1 = N + 1/2$. To evaluate $\left(\phi_N, L_\epsilon\tilde{u}^\epsilon\right)_w$, we proceed in a similar way as in $(3.18a,b)$ to obtain

$$\left(\phi_N, L_\epsilon\tilde{u}^\epsilon\right)_w \sim \epsilon w(-a)\left[\alpha - C_0(-a)^N\right]\phi_N'(-a) - \epsilon w(b)\left[\beta - C_0 b^N\right]\phi_N'(b) . \quad (4.18)$$

Then, substituting (4.9), $(4.15b)$, $(4.17a)$, and (4.18) in (4.16), we obtain the following explicit equation for C_0:

$$\begin{aligned} -\epsilon^{\nu+N+1/2}C_0(2\pi)^{1/2}g_\epsilon\, N! e^{-\epsilon^{-1}d} \sim &\left[\frac{\alpha\,\epsilon^{-N/2}}{\mathrm{He}_N(-\epsilon^{-1/2}a)} - C_0\right] a^{2N+1}\gamma_a(\epsilon)\, e^{-\epsilon^{-1}a^2/2} \\ &+ \left[\frac{\beta\,\epsilon^{-N/2}}{\mathrm{He}_N(\epsilon^{-1/2}b)} - C_0\right] b^{2N+1}\gamma_b(\epsilon)\, e^{-\epsilon^{-1}b^2/2} . \end{aligned} \quad (4.19)$$

Here $\gamma_a(\epsilon)$ and $\gamma_b(\epsilon)$ are defined in $(4.12a)$ and g_ϵ is defined in $(4.17a)$. Finally, $\tilde{u}^\epsilon$ is given in terms of C_0 by (4.14).

We note that in deriving (4.19) it was sufficient to retain only the leading order boundary layer correction terms in $\tilde{u}^\epsilon$ as given in (4.14). However, at this stage we could improve our approximation to u by adding further boundary layer correction terms to the right side of (4.14). These additional terms would be determined in by C_0. We now consider some special cases of (4.19).

Case 1: Assume that $2d > \max(a^2, b^2)$. Then, from (4.19), C_0 satisfies

$$C_0 \sim \epsilon^{-N/2} \left(\frac{\beta b^{2N+1}\gamma_b}{\mathrm{He}_N(\epsilon^{-1/2}b)} e^{\epsilon^{-1}(a^2-b^2)/2} + \frac{\alpha a^{2N+1}\gamma_a}{\mathrm{He}_N(-\epsilon^{-1/2}a)} \right) \left(b^{2N+1}\gamma_b e^{\epsilon^{-1}(a^2-b^2)/2} + a^{2N+1}\gamma_a \right)^{-1} . \tag{4.20}$$

Thus, when $b > a$ ($b < a$) we have $C_0 \sim \alpha(-a)^{-N}$ ($C_0 \sim \beta b^{-N}$) and so u has no boundary layer at $x = -a$ ($x = b$). For $|b - a| = O(\epsilon)$, (4.20) provides a uniform transition between these two limiting behaviors for C_0. Using $\mathrm{He}_N(z) = (-1)^N \mathrm{He}_N(-z)$, we have that $\gamma_a = \gamma_b$ when $a = b$. Thus, when $a = b$, (4.20) reduces to

$$C_0 \sim \frac{\epsilon^{-N/2}}{2\mathrm{He}_N(\epsilon^{-1/2}b)} \left[\beta + (-1)^N \alpha\right] \sim \frac{b^{-N}}{2} \left[\beta + (-1)^N \alpha\right] \left[1 + \frac{\epsilon}{2b^2} N(N-1)\right] . \tag{4.21}$$

Case 2: Assume that $|d - b^2/2| = O(\epsilon)$, $a > b$ and $\nu = -N - 1/2$. Then, u has boundary layers near each endpoint and C_0 satisfies

$$C_0 \sim \frac{\beta \epsilon^{-N/2}}{\mathrm{He}_N(\epsilon^{-1/2}b)} \left[1 - \frac{(2\pi)^{1/2} g_\epsilon N!}{b^{2N+1}\gamma_b} e^{-\epsilon^{-1}(d-b^2/2)}\right]^{-1} . \tag{4.22}$$

Using the leading behaviors $g_\epsilon \sim g(0)$, $\mathrm{He}_N(\epsilon^{-1/2}b) \sim \epsilon^{-N/2} b^N$ and $\gamma_b \sim 1$, we find that (4.22) reduces to the leading order result of [34]. A result similar to (4.22) holds for the case $d = a^2/2$, $b > a$ and $\nu = -N - 1/2$.

Case 3: Assume that $|d - b^2/2| = O(\epsilon)$, $b = a$ and $\nu = -N - 1/2$. Then, u has boundary layers at both endpoints, and (4.19) becomes

$$C_0 \sim \frac{\epsilon^{-N/2}}{\mathrm{He}_N(\epsilon^{-1/2}b)} \left[\beta + (-1)^N \alpha\right] \left[2 - \frac{(2\pi)^{1/2} g_\epsilon N!}{b^{2N+1}\gamma_b} e^{-\epsilon^{-1}(d-b^2/2)}\right]^{-1} . \tag{4.23}$$

4.3 Examples and Computations

We now consider some specific examples and we verify the asymptotic results with corresponding numerical results.

Example 4.1: For $b > 0$, consider

$$\epsilon u'' - x u' + u = s(2\pi)^{-1/2} \epsilon^{-3/2} e^{-\epsilon^{-1} d} u , \quad -1 \le x \le b ; \qquad u(-1) = 1 , \quad u(b) = 2 . \tag{4.24}$$

This problem was studied in [14] when $b = 1$ and $s = 0$ and it was considered in [29] and [30] for arbitrary b and $s = 1$. From (4.14), the composite expansion for the solution to (4.24) is

$$\tilde{u}^\epsilon(x) = (1 + C_0)\, e^{-\epsilon^{-1}(1+x)} + (2 - C_0 b)\, e^{-b\epsilon^{-1}(b-x)} + C_0 x , \tag{4.25}$$

where C_0 satisfies (4.19). We first consider the case $s = 0$. Then from (4.12b) and (4.20), we find that C_0 satisfies

$$C_0 \sim \frac{2b^2 \rho_\epsilon(b)\, e^{\epsilon^{-1}(1-b^2)/2} - 1}{b^3 \rho_\epsilon(b)\, e^{\epsilon^{-1}(1-b^2)/2} + 1}\,, \qquad \rho_\epsilon(b) \sim \frac{1 - 3\epsilon b^{-2}}{1 - 3\epsilon}\,. \tag{4.26}$$

This result for C_0 is easily verified by expanding, for $\epsilon \to 0$, the exact solution to (4.24) (with $s = 0$) given by

$$\begin{aligned} u(x) &= a_1 x + a_2 \left(e^{\epsilon^{-1}x^2/2} - \epsilon^{-1} x\, J_\epsilon(x) \right)\,, \qquad J_\epsilon(x) \equiv \int_{-1}^{x} e^{\epsilon^{-1}s^2/2}\, ds\,, \\ a_2 &= (2+b) \left[b e^{\epsilon^{-1}/2} + e^{\epsilon^{-1}b^2/2} - \epsilon^{-1} b J_\epsilon(b) \right]^{-1}\,, \qquad a_1 = -1 + e^{\epsilon^{-1}/2}\, a_2\,. \end{aligned} \tag{4.27}$$

For $\epsilon = 1/60$ and $s = 0$, in Table 5a we compare the numerical value of C_0 with the asymptotic result (4.26) as b is varied in a narrow range near $b = 1$. The numerical value of C_0 is defined by $C_0 = u'(0)$, where u is computed from (4.24) using the method of [21]. From (4.13), we calculate that $\lambda_0 \approx -3.3 \times 10^{-11}$, when $b = 1$ and $\epsilon = 1/60$. Despite this ill-conditioning, the asymptotic and numerical results in Table 5a agree to several decimal places of accuracy. For three values of ϵ, in Fig. 4 we plot $C_0 = C_0(b)$ obtained from the asymptotic result (4.26). In this figure we also show the numerical results for C_0 for the case $\epsilon = 1/60$.

Now let $s = 1$ and $|d - b^2/2| = O(\epsilon)$ with $b < 1$. Then, since $g_\epsilon = -(2\pi)^{-1/2}$, (4.12$b$) and (4.22) provide

$$C_0 \sim 2b^2 \left[b^3 + \left(1 - \frac{3\epsilon}{b^2}\right)^{-1} e^{-\epsilon^{-1}(d - b^2/2)} \right]^{-1}\,. \tag{4.28}$$

Thus, when $d = b^2/2$, we have $C_0 \sim 2(b^3+1)^{-1} \left[b^2 - 3\epsilon(b^3+1)^{-1} \right]^{-1}$, which agrees with the two term result in [30] that was obtained using an extension of the variational method. Finally, when $b = 1$ and $d - 1/2 = O(\epsilon)$, we obtain from (4.23) that

$$C_0 \sim \left[2 + (1 - 3\epsilon)^{-1} e^{-\epsilon^{-1}(d - 1/2)} \right]^{-1}\,. \tag{4.29}$$

Setting $d = b^2/2$ and $s = 1$, in Tables 5b and 5c we show the very close agreement between the asymptotic and numerical values for C_0 as a function of ϵ for the cases $b = 1$ and $b = 3/4$, respectively. Setting $b = 1$ and $\epsilon = 1/60$, in Table 5d we compare C_0 values as d is varied in a narrow region near $d = 1/2$. A plot of $C_0 = C_0(d)$ for $\epsilon = 1/60$ is shown in Fig. 5. In Fig. 5 we also plot the numerical solution to (4.24) at a few values of d. In Table 5e we compare C_0 for various d for the case $b = 3/4$ and $\epsilon = 1/100$.

Example 4.2: Our next example is

$$\epsilon u'' - x u' + N u = -s\, \frac{(2\pi)^{-1/2} \epsilon^{-N-1/2}}{[(x+1)^2 + 1]}\, e^{-\epsilon^{-1} d}\, u\,, \quad -1 \le x \le b\,; \qquad u(-1) = 1\,, \quad u(b) = 2\,, \tag{4.30}$$

with $b > 0$. The composite expansion is given in (4.14) with $\alpha = 1$, $\beta = 2$ and $a = 1$. For several parameter ranges we now give results for C_0 obtained from (4.19) – (4.23). When $s = 0$, then

$$C_0 \sim \frac{2b^{N+1} \rho_\epsilon(b)\, e^{\epsilon^{-1}(1-b^2)/2} + (-1)^N \rho_\epsilon(1)}{b^{2N+1} \eta_\epsilon(b)\, e^{\epsilon^{-1}(1-b^2)/2} + \eta_\epsilon(1)}\,, \tag{4.31}$$

where $\rho_\epsilon(b) \sim 1 - \epsilon b^{-2}(N+1)(N+2)/2$ and $\eta_\epsilon(b) \sim 1 - \epsilon b^{-2}(N^2+N+1)$ as $\epsilon \to 0$. Setting $s = 0$ and $\epsilon = 1/60$, in Table 6a we show the close agreement between the asymptotic and numerical values of C_0 as b is varied near $b = 1$. Note that the numerical value of C_0 is now defined by $C_0 = -\epsilon^{-1}u(0)$, where $u(0)$ is obtained from the numerical solution to (4.30).

Now when $s = 1$, $|d - b^2/2| = O(\epsilon)$ and $b < 1$,

$$C_0 \sim 4b^{-N}\left(1 - \frac{\epsilon N(N-1)}{2b^2}\right)^{-1}\left[2 - b^{-2N-1}\zeta_\epsilon(b)N!\,e^{-\epsilon^{-1}(d-b^2/2)}\right]^{-1}. \tag{4.32}$$

Finally, when $s = 1$, $|d - 1/2| = O(\epsilon)$ and $b = 1$,

$$C_0 \sim 2\left(1 - \frac{\epsilon N(N-1)}{2}\right)^{-1}\left(2 + (-1)^N\right)\left[4 - \zeta_\epsilon(1)N!\,e^{-\epsilon^{-1}(d-1/2)}\right]^{-1}. \tag{4.33}$$

In (4.32) and (4.33), $\zeta_\epsilon(b)$ is given by

$$\zeta_\epsilon(b) \sim \frac{1 + \epsilon(N + 1/2)}{1 - \epsilon(N^2 + N + 1)b^{-2}}. \tag{4.34}$$

Setting $d = 1/2$, $b = 1$ and $s = 1$, in Table 6b we show the favorable agreement between the asymptotic and numerical values for C_0 as ϵ is decreased. Setting $b = 1$ and $\epsilon = 1/60$, in Table 6c we compare C_0 values as d is varied near $d = 1/2$. For the case $b = 3/4$ and $\epsilon = 1/100$, in Fig. 6 we compare the asymptotic and numerical results for $C_0 = C_0(d)$ when d is near $9/32$. Numerical values for $C_0(d)$ are given in Table 6d. In Fig. 6 we also plot the numerical solution to (4.30) at a few values of d. From this figure, we note that as d increases past $9/32$, the boundary layer near the right endpoint disappears.

There are two main conclusions to be drawn from the examples considered in §3 and §4. Firstly, the asymptotic results given for C_0 typically provide a very close determination of the numerical value, even when considering the delicate transition behavior in C_0 as certain parameters, such as d, cross through critical values. However, we emphasize that to obtain a close quantitative agreement between the asymptotic and numerical values for C_0 at a small but finite ϵ, it is crucial to obtain at least a two term expansion for the pre-exponential factors in the asymptotic formulas for C_0. These expansions, which were derived in §3 and §4, extend some previous leading order analytical results for C_0 that were obtained using the variational principle of [9]. Our second conclusion is that, provided that λ_0 is not exceedingly small, the numerical method of [21] provides accurate numerical solutions to these highly ill-conditioned problems. Moreover, the numerical method is able to determine the change in C_0 that occurs as a result of exponentially small changes in the coefficient of the differential operator. Thus, for certain ranges of ϵ, the numerical results can be reliably used to verify the corresponding asymptotic results.

5. Extensions of the Theory

In §5.1 we examine some inhomogeneous problems and in §5.2 we apply the results to a model equation arising from the shape from shading problem.

5.1 The Inhomogeneous Problem

Hermite Operator: We now consider a forced version of (4.1) given by

$$L_\epsilon u \equiv \epsilon u'' - xu' + Nu = g(x)\epsilon^\nu e^{-\epsilon^{-1}d}\,, \qquad -a \le x \le b\,, \qquad u(-a) = \alpha\,, \qquad u(b) = \beta\,. \tag{5.1}$$

Here $d > 0$, N is a non-negative integer and $g(x)$ is a smooth function. Since $d > 0$, the composite expansion $\tilde{u}^\epsilon$ for the solution to (5.1) is given by (4.14) where C_0 is to be found. To determine C_0 we use the projection method. Substituting $v = u - \tilde{u}^\epsilon$ in (5.1) and expanding v in terms of the eigenfunctions ϕ_j of $L_\epsilon\phi = \lambda\phi$, we obtain

$$v = \sum_{j=0}^{\infty} \frac{A_j}{\lambda_j}\phi_j\,, \qquad A_j = \epsilon w v \phi_j' \Big|_{-a}^{b} - \left(\phi_j, L_\epsilon \tilde{u}^\epsilon\right)_w + \epsilon^\nu e^{-\epsilon^{-1}d}\left(\phi_j, g\right)_w\,, \tag{5.2}$$

where $w = e^{-\epsilon^{-1}x^2/2}$. The limiting solvability condition $A_N = 0$ then gives the following equation for C_0:

$$\epsilon^\nu e^{-\epsilon^{-1}d}\left(\phi_N, g\right)_w = \left(\phi_N, L_\epsilon \tilde{u}^\epsilon\right)_w - \epsilon w v \phi_N' \Big|_{-a}^{b}\,. \tag{5.3}$$

Since the right side of (5.3) was evaluated in §4.2, we need only calculate the left side of (5.3). Using $\phi_N \sim M_N \mathrm{He}_N(\epsilon^{-1/2}x)$ and the orthogonality properties of the Hermite polynomials, we readily calculate that

$$\left(\phi_N, g\right)_w \sim M_N \epsilon^{(N+1)/2}\left(2\pi\right)^{1/2} g_\epsilon\,, \qquad g_\epsilon \sim \sum_{j=0}^{\infty} \epsilon^j\,\theta_j\,g^{(N+2j)}(0)\,. \tag{5.4a}$$

Here θ_j is defined by

$$\theta_j = \frac{(2\pi)^{-1/2}}{(N+2j)!}\int_{-\infty}^{\infty} z^{2j+N}\mathrm{He}_N(z)e^{-z^2/2}\,dz\,. \tag{5.4b}$$

In particular, $\theta_0 = 1$ and $\theta_1 = 1/2$. Substituting (4.9), (4.15*b*), (4.18) and (5.4) in (5.3), we obtain an equation for C_0 that can be solved to yield

$$C_0 \sim C_{0H} - \frac{(2\pi)^{1/2} g_\epsilon\,\epsilon^{\nu+N+1/2}\,e^{-\epsilon^{-1}(d-a^2/2)}}{a^{2N+1}\gamma_a(\epsilon) + b^{2N+1}\gamma_b(\epsilon)\,e^{\epsilon^{-1}(a^2-b^2)/2}}\,. \tag{5.5}$$

Here $\gamma_a(\epsilon)$ and $\gamma_b(\epsilon)$ are defined in (4.12*a*), and C_{0H} is defined to be the right side of (4.20). The asymptotic solution to (5.1) is then given in terms of C_0 by (4.14). Notice that $C_0 \sim C_{0H}$ when $g(x) = 0$.

We now make some remarks concerning (5.1). Suppose that $b = a$, $\nu = -N - 1/2$ and $g^{(N)}(0) \neq 0$. Then from (5.5) and (5.1) we conclude that a forcing of order $O\left(\epsilon^{-N-1/2}e^{-\epsilon^{-1}d}\right)$ produces an exponentially larger response in u of order $O\left(e^{-\epsilon^{-1}(d-b^2/2)}\right)$. In particular, if $d = b^2/2$ the forcing induces an $O(1)$ response. This exponential sensitivity is simply another manifestation of the exponential ill-conditioning of the underlying problem. Notice, however, that if $g(x)$ is a polynomial of degree $N-1$ then $\left(\phi_N, g\right)_w$ is exponentially small. For this special form of $g(x)$, it can be shown that the solution to (5.1) is not exponentially sensitive to an exponentially small forcing. We now consider a specific example.

Example 5.1: Consider (5.1) with $\beta = 2$, $\alpha = 1$, $a = 1$, $N = 2$, $\nu = -5/2$ and $g(x) = (2\pi)^{-1/2}(1+x^2)^{-1}$. Then, using (4.12$b$), (4.20) and (5.4), (5.5) becomes

$$C_0 \sim \frac{2b^3(1-6\epsilon b^{-2})\, e^{\epsilon^{-1}(1-b^2)/2} + (1-6\epsilon) + (2-12\epsilon)\, e^{-\epsilon^{-1}(d-1/2)}}{b^5(1-7\epsilon b^{-2})\, e^{\epsilon^{-1}(1-b^2)/2} + (1-7\epsilon)} \,. \tag{5.6}$$

Therefore, when $b = 1$ and $d = 1/2$ then $C_0 \sim 5(1+\epsilon)/2$. Setting $b = 1$ and $d = 1/2$, in Table 7a we compare the asymptotic and numerical values for C_0 as ϵ is decreased. The numerical value of C_0 is defined by $C_0 = -\epsilon^{-1}u(0)$, where $u(0)$ is computed from (5.1). In Table 7b we fix $\epsilon = 1/60$ and $b = 1$ and we compare values for $C_0 = C_0(d)$ as d is varied in a neighborhood of $d = 1/2$. In Fig. 7 we plot $C_0 = C_0(d)$ and we show the numerical solution to (5.1) at a few values of d.
Exit Operator: We now consider a forced version of (3.1) given by

$$\begin{aligned} &L_\epsilon u \equiv \epsilon u'' - x^{2m+1}p(x)u' = g(x)\epsilon^\nu e^{-\epsilon^{-1}d}\,, \qquad -a \le x \le b\,, \\ &u(-a) = \alpha\,, \qquad u(b) = \beta\,. \end{aligned} \tag{5.7}$$

Here $d > 0$, $g(x)$ and $p(x) > 0$ are smooth functions and m is a non-negative integer. Since $d > 0$, the composite expansion for the solution to (5.7) is given by (3.13) where C_0 is to be found. Using the projection method, we readily find that C_0 satisfies

$$C_0 \sim C_{0H} - \frac{\epsilon^{\nu+1/(2m+2)}\, g_\epsilon\, e^{-\epsilon^{-1}(d-\omega_{-a})}}{a^{2m+1}p(-a)\gamma_a(\epsilon) + b^{2m+1}p(b)\gamma_b(\epsilon)\, e^{-\epsilon^{-1}(\omega_b-\omega_{-a})}} \,. \tag{5.8}$$

Here g_ϵ is defined in (3.17a), $\gamma_a(\epsilon)$ and $\gamma_b(\epsilon)$ are defined in (3.8) while ω_{-a} and ω_b are defined in (3.10b). In (5.8), C_{0H} is the value of C_0 for the homogeneous problem and is defined as the right side of (3.20). Thus, in analogy with the forced Hermite problem (5.1), the solution to (5.7) can be exponentially sensitive to an exponentially small forcing function. However, we note that in the special case when $g(x)$ is odd, the coefficient of order $O(\epsilon^{j/(m+1)})$ in the expansion of g_ϵ vanishes for any $j \ge 0$. It then follows that $\left(\phi_0, g\right)_w$ is exponentially small and, consequently, the exponential sensitivity of the solution to (5.7) is suppressed.

Example 5.2: In (5.7) let $\beta = 2$, $\alpha = 1$, $b = a = 1$, $m = 0$, $\nu = -1/2$, $p(x) = 2\pi x^{-1}\sin(\pi x/2)$ and $g(x) = 1 + x^2$. Then, using (3.8), (3.10b) and (3.17a), (5.8) becomes

$$C_0 \sim \frac{3}{2} - \left(\frac{2}{\pi}\right)^{1/2} \frac{e^{\epsilon^{-1}(4-d)}}{4\pi} \left[1 + \epsilon\left(\frac{1}{\pi^2} + \frac{1}{32}\right)\right] . \tag{5.9}$$

5.2 An Exponentially Ill-Conditioned Diffusive Regularization

Following [4], we now consider the forced problem

$$N_\epsilon y \equiv -\epsilon\, y'' + 2yy' = f(x,\epsilon)\,, \quad -1 \le x \le 1\,, \quad y(-1) = \pi\,,\ y(1) = -\pi\,. \tag{5.10}$$

This BVP, which is a model problem illustrating the effect of a diffusive regularization on the more general shape from shading problem, was studied numerically in [4]. A discussion of the shape from shading problem and the specific motivation for considering (5.10) are described in [4].

Let $y_0(x)$ be an odd, monotone non-increasing, function that is independent of ϵ and that satisfies the boundary conditions in (5.10). In [4], the forcing f in (5.10) was chosen as $f = f_0 \equiv 2y_0 y_0^{'}$ where y_0 can assume either of the two forms

$$y_0(x) = \pi \cos\left[\frac{\pi}{2}(x+1)\right] , \quad (\text{type A}) ; \qquad y_0(x) = -\pi x^3 , \quad (\text{type B}) . \tag{5.11}$$

For each of these two forms of $y_0(x)$, the term $\epsilon y_0^{''}$ is uniformly small throughout the domain as $\epsilon \to 0$. Therefore, it seems reasonable to expect that the solution to (5.10) with f replaced by f_0 will satisfy $|y - y_0(x)| = O(\epsilon)$ uniformly on $[0,1]$. In the sense it was hoped in [4] that the $\epsilon y^{''}$ term in (5.10) is a diffusive regularization of the first order equation $2yy^{'} = f$. We note that, since y is assumed to have a zero-crossing, this reduced problem requires some type of regularization. Rather interestingly, the computations in [4] using (5.10) and (5.11) showed that the solution to the regularized problem differs significantly from y_0 even when ϵ is rather small. This difference is most pronounced near the turning point region at $x = 0$. Moreover, a rather large number of Newton iterations were required for numerical convergence of the discrete scheme used for (5.10), and in several instances convergence was not obtained.

We suggest that the qualitative effect of this diffusive regularization can largely be understood by studying the operator associated with linearizing (5.10) about $y_0(x)$. In what follows, we make y_0 be an *exact* solution to (5.10) by choosing $f = f_0 \equiv N_\epsilon y_0$. For $\epsilon \to 0$, we then show that if f is perturbed from f_0 by an *exponentially small* amount, the solution to (5.10) can deviate from y_0 by an *algebraically* small amount. This exponential sensitivity in response to very small changes in the forcing function occurs as a result of the exponential ill-conditioning of the linearized operator.

We now perform such a sensitivity analysis for

$$N_\epsilon y \equiv -\epsilon\, y^{''} + 2yy^{'} = f_0(x,\epsilon) + \epsilon^\nu e^{-\epsilon^{-1}d}\, g(x) , \quad -1 \le x \le 1 , \quad y(\pm 1) = \mp\pi , \tag{5.12}$$

where $f_0 = N_\epsilon y_0$ and y_0 is given in (5.11). In (5.12), $\nu > 0$, $g(x)$ is smooth, and d is a positive constant to be specified below. Setting $y = y_0 + v$ in (5.12), we obtain the following linearized problem for v:

$$\epsilon v^{''} - 2\,(y_0 v)^{'} = -\epsilon^\nu\, e^{-\epsilon^{-1}d} g(x) , \quad -1 \le x \le 1 , \quad v(\pm 1) = 0 . \tag{5.13}$$

Now introduce u by $v = wu$, where $w = w(x,\epsilon) \equiv \exp\left[2\epsilon^{-1}\int_0^x y_0(\eta)\, d\eta\right]$. Then, from (5.13), we find that u satisfies

$$L_\epsilon u \equiv \epsilon u^{''} + 2y_0 u^{'} = -\epsilon^\nu e^{-\epsilon^{-1}d} w^{-1}\, g(x) , \quad -1 \le x \le 1 , \quad u(\pm 1) = 0 . \tag{5.14}$$

Clearly, (5.14) with (5.11) is an example of (5.7). Let λ_0 be the exponentially small eigenvalue of $L_\epsilon \phi = \lambda\phi$ with $\phi(\pm 1) = 0$. Then, for y_0 of type A, λ_0 was given in (3.12*a*), whereas for y_0 of type B, λ_0 was given in (3.12*c*). Using the projection method, we can solve (5.14) for u and then recover y from $y = y_0 + uw$. This calculation leads to

$$y \sim y_0(x) + C_0 \left(1 - e^{-2\pi\epsilon^{-1}(1+x)} - e^{-2\pi\epsilon^{-1}(1-x)}\right) \exp\left(2\epsilon^{-1} \int_0^x y_0(\eta)\, d\eta\right) , \tag{5.15a}$$

where C_0 satisfies

$$C_0 \sim \frac{\epsilon^{\nu}}{4\pi} \exp\left[-\epsilon^{-1}(d-\gamma)\right] \int_{-1}^{1} g(\eta)\, d\eta\,, \qquad \text{with} \qquad \gamma = -2\int_0^1 y_0(\eta)\, d\eta\,. \tag{5.15b}$$

For y_0 of type A, $\gamma = 4$ and for y_0 of type B, $\gamma = \pi/2$. It is clear from (5.15) that, in general, our linearization assumption is only valid when $d \geq \gamma$. Note that if $d = \gamma$, this assumption requires that $\nu > 0$.

Comparing (5.15) with (5.12), and noting that $w = \exp\left(2\epsilon^{-1}\int_0^x y_0(\eta)\, d\eta\right)$ is strongly concentrated near $x = 0$, we conclude that a perturbation in the forcing of order $O\left(\epsilon^{\nu} e^{-\epsilon^{-1}\gamma}\right)$ can perturb the solution near the turning point region by an amount of order $O(\epsilon^{\nu})$ unless $\int_{-1}^{1} g(\eta)\, d\eta = 0$. Since w is exponentially small away from $x = 0$, this perturbation in the forcing does not have nearly such a dramatic effect on the solution away from the turning point region.

We remark that if $0 < d < \gamma$, our linearization assumption is not valid. However, in this case, (5.15) certainly leads to the conjecture that y can differ substantially from y_0 near the turning point region. Although our sensitivity analysis does not precisely explain the numerical findings of [4] obtained from the discrete form of (5.10), this analysis does show, at least at the continuous level, the severe ill-conditioning that can be associated with (5.10).

As an example, consider (5.13) – (5.15) for $g(x) = 1$, and for $y_0(x)$ of type A. Without loss of generality we can take $\nu = 0$. For $\epsilon = 1/8$, in Table 7c and Fig. 8 we compare the asymptotic and numerical values for $C_0 = C_0(d)$ for d near $\gamma = 4$. In Fig. 8 we also plot, at several values of d, the numerical solutions $u(x)$ and $v(x)$ to (5.14) and (5.13), respectively. Although the computed solutions for $d < 4$ are not strictly relevant to the sensitivity analysis above, it is clear from Fig. 8 that the spike type behavior in $v = y - y_0$ near the turning point region becomes more pronounced as d is decreased.

6. Nonlinear Problems with Exponentially Ill-Conditioned Linearizations

We now consider some nonlinear problems that are associated with small eigenvalues.

6.1 Eigenvalues for Linearized Viscous Shock Problem

Consider the viscous shock problem

$$u_t + [f(u)]_x = \epsilon u_{xx}\,, \qquad 0 \leq x \leq 1\,, \tag{6.1a}$$

$$\epsilon u_x(0,t) - \kappa_l\left[u(0,t) - \alpha\right] = 0\,, \qquad \epsilon u_x(1,t) + \kappa_r\left[u(1,t) + \alpha\right] = 0\,, \tag{6.1b}$$

where $\kappa_l > 0$, $\kappa_r > 0$ and $\alpha > 0$. We assume that $(\kappa_r - \alpha)(\kappa_l - \alpha) > 0$ and that $f(u)$ is a convex function satisfying $f(0) = f'(0) = 0$ and $f(\alpha) = f(-\alpha)$. This problem, and various related problems with special forms of $f(u)$, have been analyzed for $\epsilon \to 0^+$ in [18], [27], [28], [19] and [20]. These analyses have uncovered three main features for the solution to (6.1). Firstly, (6.1) has an equilibrium shock layer solution $u^e = u^e(x,\epsilon)$ where the shock layer location x_0^{ϵ}, defined by $u^e(x_0^{\epsilon},\epsilon) = 0$ and satisfying $0 < x_0^{\epsilon} < 1$, can only be determined by resolving exponentially small effects. Secondly, there is an exponentially slow shock layer motion for the evolution problem. Thirdly, the linearization of (6.1) around $u^e(x,\epsilon)$ is exponentially ill-conditioned. For a certain parameter range, an asymptotic estimate for the exponentially small eigenvalue was given in [27]. We now give further eigenvalue estimates for other parameter ranges and we relate (6.1) to the exit problem (3.1). More importantly, the eigenvalue estimates are verified numerically for Burgers equation.

The linearization of (6.1a) around u^e leads to the eigenvalue problem

$$\epsilon\, v_{xx} + [q(x,\epsilon)v]_x = \lambda v\,, \qquad q(x,\epsilon) \equiv -f^{'}[u^e(x,\epsilon)]\,. \tag{6.2}$$

Thus, defining $v = \exp\left[-\epsilon^{-1}Q(x,\epsilon)\right]\phi$ where $Q(x,\epsilon) \equiv \int_{x_0^e}^{x} q(\eta,\epsilon)\,d\eta$, we obtain

$$L_\epsilon \phi \equiv \epsilon\, \phi_{xx} - q(x,\epsilon)\phi_x = \lambda\phi\,, \tag{6.3a}$$

$$\epsilon\, \phi_x(0) - [\kappa_l + q(0,\epsilon)]\,\phi(0) = 0\,, \qquad \epsilon\,\phi_x(1) + [\kappa_r - q(1,\epsilon)]\,\phi(1) = 0\,. \tag{6.3b}$$

Since $q(x_0^e,\epsilon) = 0$, $q_x(x_0^e,\epsilon) > 0$ and $(x - x_0^e)q(x,\epsilon) > 0$ for $0 < x < 1$, (6.3) has the form of the exit operator (3.1) with $m = 0$ and with the turning point at x_0^e rather than at $x = 0$. Thus, (6.3) has an eigenpair ϕ_0, λ_0 where λ_0 is exponentially small and where $\phi_0 \sim 1$ away from boundary layers near $x = 0$ and $x = 1$.

To calculate λ_0 we use the following identity:

$$\lambda_0 \left(\phi_0, 1\right)_w = [q(1,\epsilon) - \kappa_r]\,\phi_0(1)w(1) - [q(0,\epsilon) + \kappa_l]\,\phi_0(0)w(0)\,. \tag{6.4}$$

Here $\left(u,v\right)_w \equiv \int_0^1 uvw\,dx$ and $w = \exp\left[-\epsilon^{-1}Q(x,\epsilon)\right]$. Then, from a boundary layer analysis, we derive that $\phi_0(1) \sim q(1,\epsilon)/\kappa_r$ and $\phi_0(0) \sim -q(0,\epsilon)/\kappa_l$. Therefore, (6.4) becomes

$$\lambda_0 \int_0^1 \exp\left[-\epsilon^{-1}Q\right]\,dx \sim \left[\frac{q(1,\epsilon)}{\kappa_r} - 1\right] q(1,\epsilon)\,e^{-\epsilon^{-1}Q(1,\epsilon)} + \left[\frac{q(0,\epsilon)}{\kappa_l} + 1\right] q(0,\epsilon)e^{-\epsilon^{-1}Q(0,\epsilon)}\,. \tag{6.5}$$

Here $Q(x,\epsilon)$ was defined following (6.2). We note that $q(x,\epsilon) = -f^{'}(\mp\alpha) + O\left(e^{-C_\pm}\right)$ as $\epsilon^{-1}(x - x_0^e) \to \pm\infty$ for some $C_\pm > 0$. Thus, in contrast to the situation in §3.1, for (6.3) there are no higher order boundary layer correction terms for ϕ_0 near $x = 0$ and $x = 1$ that are algebraic in ϵ.

Consider Burgers equation where $f(u) = u^2/2$. In this case,

$$u^e(x) = -\beta\tanh\left[\beta\epsilon^{-1}(x - x_0^e)/2\right] = -q(x,\epsilon)\,, \qquad Q(x,\epsilon) = 2\epsilon\log\left(\cosh\left[\beta\epsilon^{-1}(x - x_0^e)/2\right]\right)\,, \tag{6.6}$$

where β and x_0^e satisfy the transcendental equations

$$\begin{aligned} \beta^2\mathrm{sech}^2\left(\beta\epsilon^{-1}x_0^e/2\right) + 2\kappa_l\left[\beta\tanh\left(\beta\epsilon^{-1}x_0^e/2\right) - \alpha\right] &= 0\,, \\ \beta^2\mathrm{sech}^2\left[\beta\epsilon^{-1}(1 - x_0^e)/2\right] + 2\kappa_r\left[\beta\tanh\left(\beta\epsilon^{-1}(1 - x_0^e)/2\right) - \alpha\right] &= 0\,. \end{aligned} \tag{6.7}$$

Thus, the integral on the left side of (6.5) satisfies $\int_0^1 \exp\left[-\epsilon^{-1}Q\right]dx \sim 4\epsilon\beta^{-1} + \text{T.S.T.}$ as $\epsilon \to 0$.

We now give asymptotic estimates for λ_0, calculated from (6.5)–(6.7), for four different ranges of κ_l and κ_r. First, let $\kappa_l = \kappa_r \equiv \kappa \neq \alpha$. Then, $x_0^e = 1/2$, $\beta \sim \alpha + 2\alpha(1 - \alpha/\kappa)e^{-\alpha\epsilon^{-1}/2}$ and

$$\lambda_0 \sim 2\epsilon^{-1}\alpha^2\left(\frac{\alpha}{\kappa} - 1\right)e^{-\epsilon^{-1}\alpha/2}\,, \qquad (\kappa \neq \alpha)\,. \tag{6.8}$$

Now, let $\kappa_l = \kappa_r \equiv \kappa = \alpha$. Then, $x_0^e = 1/2$, $\beta \sim \alpha + 2\alpha e^{-\epsilon^{-1}\alpha}$ and

$$\lambda_0 \sim -4\epsilon^{-1}\alpha^2 e^{-\epsilon^{-1}\alpha}\,, \qquad (\kappa = \alpha)\,. \tag{6.9}$$

Next, let $\kappa_l = \infty$ and $\kappa_r > \alpha$. Then, $x_0^e \sim 1/2 - \epsilon(2\alpha)^{-1}\log(1-\alpha/\kappa_r)$, $\beta \sim \alpha + 2\alpha e^{-\epsilon^{-1}\alpha x_0^e}$ and

$$\lambda_0 \sim -2\epsilon^{-1}\alpha^2\left(1-\alpha/\kappa_r\right)^{1/2} e^{-\epsilon^{-1}\alpha/2}\,, \qquad (\kappa_l = \infty\,,\ \kappa_r > \alpha)\,. \tag{6.10}$$

Finally, let $\kappa_l = \infty$ and $\kappa_r = \alpha$. Then $x_0^e \sim 2/3 + \text{T.S.T.}$, $\beta \sim \alpha + 2\alpha e^{-2\epsilon^{-1}\alpha/3}$ and

$$\lambda_0 \sim -3\epsilon^{-1}\alpha^2 e^{-2\epsilon^{-1}\alpha/3}\,, \qquad (\kappa_l = \infty\,,\ \kappa_r = \alpha)\,. \tag{6.11}$$

The result (6.8) was given in [27]. Comparing (6.8) with (6.9) and (6.10) with (6.11) we note that the estimate for λ_0 changes significantly as κ_r (or κ_l) crosses through α. It is significantly more difficult to provide estimates for λ_0 that uniformly incorporate these transitions.

Before comparing (6.8) – (6.11) with corresponding numerical results for λ_0, we formulate two eigenvalue problems that, for Burgers equation, are equivalent to (6.3). These equivalent problems are introduced primarily to illustrate the flexibility of the eigenvalue solver of [21] for accurately computing the spectrum associated with different types of singularly perturbed Sturm Liouville operators. The first equivalent problem is obtained by substituting $\psi = \exp\left[-Q/2\epsilon\right]\phi$ in (6.3), where Q is defined in (6.6). We then obtain

$$\begin{gathered}\epsilon^2\psi_{xx} + \frac{\beta^2}{2}\,\text{sech}^2\left[\frac{\beta\epsilon^{-1}}{2}(x-x_0^e)\right]\psi = \left(\epsilon\lambda + \frac{\beta^2}{4}\right)\psi\,, \qquad 0<x<1 \\ \epsilon\psi_x(1) + [\kappa_r - \frac{1}{2}q(1,\epsilon)]\psi(1) = 0\,, \qquad \epsilon\psi_x(0) - [\kappa_l + \frac{1}{2}q(0,\epsilon)]\psi(0) = 0\,.\end{gathered} \tag{6.12}$$

The problem (6.12) can also be recast using the transformation $\xi = \tanh\left[\beta\epsilon^{-1}(x-x_0^e)/2\right]$ and $\varphi(\xi) = \psi[x(\xi)]$ to the following Legendre's equation with eigenvalue parameter $\mu^2 = 1 + 4\epsilon\lambda\beta^{-1}$:

$$\left[(1-\xi^2)\varphi_\xi\right]_\xi + 2\varphi = \mu^2\left(1-\xi^2\right)^{-1}\varphi\,, \qquad -\xi_l < \xi < \xi_r\,, \tag{6.13a}$$

$$\varphi_\xi(\xi_r) + F_\epsilon\left(1-x_0^e,\kappa_r\right)\varphi(\xi_r) = 0\,, \qquad \varphi_\xi(-\xi_l) - F_\epsilon\left(x_0^e,\kappa_l\right)\varphi(-\xi_l) = 0\,. \tag{6.13b}$$

Here ξ_l, ξ_r and F_ϵ are defined by $\xi_l = -\tanh\left(\beta\epsilon^{-1}x_0^e/2\right)$, $\xi_r = \tanh\left[\beta\epsilon^{-1}(1-x_0^e)/2\right]$ and

$$F_\epsilon(a_1,a_2) = \frac{2}{\beta}\cosh^2\left(\frac{\beta\epsilon^{-1}a_1}{2}\right)\left[a_2 - \frac{\beta}{2}\tanh\left(\frac{\beta\epsilon^{-1}a_1}{2}\right)\right]\,. \tag{6.13c}$$

Since λ_0 is exponentially small, then (6.13) has an eigenvalue with μ exponentially close to one.

The eigenvalue solver of [21] allows for accurate numerical computations of λ_0 using any one of the three equivalent formulations (6.3), (6.12) or (6.13). In particular, the method can compute the spectrum associated with a strongly localized potential such as in (6.12) and the method can also treat nearly singular Sturm Liouville operators such as in (6.13). Notice, in (6.13), that since the endpoints ξ_l and ξ_r are exponentially close to the regular singular points $\xi = \pm 1$, it would certainly be difficult, using standard numerical methods, to accurately compute the eigenvalue μ with μ exponentially close to one.

To compute λ_0 numerically in various cases, we first accurately solve (6.7) for x_0^e and β using Newton's method. The eigenvalue solver of [21] is then used to compute λ_0 from either (6.3), (6.12) or (6.13). In the computations below we set $\alpha = 1$. In Tables 8a, 8b, 8c and 8d we compare the asymptotic and numerical values for λ_0 for different parameter values corresponding to (6.8), (6.9), (6.10) and (6.11), respectively. From these tables we observe that the asymptotic result closely determines λ_0 even at moderately small values of ϵ. Note that in each table there is a range of ϵ where the numerically computed value of λ_0 differs from the asymptotic value of λ_0 by roughly 10^{-13}. This suggests not only that the asymptotic results for λ_0 are very precise but also that the numerical method of [21] gives accurate results for λ_0 to within roughly 13 decimal places.

As a remark, for the case $\kappa_r = \kappa_l = \infty$, $\alpha = 1$ and $\epsilon = 1/50$, the result $\lambda_0 = -1.24 \times 10^{-9}$ was computed in [18] using a finite difference method. This is to be contrasted with the result $\lambda_0 = -1.38879 \times 10^{-9}$ that was computed using the method of [21]. From (6.8) the asymptotic result is $\lambda_0 = -1.38876 \times 10^{-9}$.

6.2 The Linearized Allen-Cahn Equation

Consider the boundary value problem $\epsilon^2 u_{xx} + 2(u - u^3) = 0$ on $0 \le x \le 1$ with $u_x(0) = u_x(1) = 0$. A monotonically increasing solution to this problem with exactly one internal layer is given, to within exponentially small terms, by $u(x, \epsilon) = \tanh[\epsilon^{-1}(x - 1/2)]$. Linearizing around this solution we obtain the following eigenvalue problem, which is closely related to (6.12):

$$\epsilon^2 v_{xx} + 6\,\mathrm{sech}^2\left[\epsilon^{-1}(x - \frac{1}{2})\right] v = \big(\lambda + 4\big) v\,, \qquad v_x(0) = v_x(1) = 0\,. \tag{6.14}$$

For this problem, the first eigenvalue λ_0 satisfies $\lambda_0 \sim 96\, e^{-2\epsilon^{-1}}$ as $\epsilon \to 0$ (see [32]). In Table 8e we show the close agreement between this asymptotic result for λ_0 and the corresponding numerical result for λ_0 computed from (6.14).

6.3 An Ill-Conditioned System

Exponentially ill-conditioned linearizations can also be associated with systems of boundary value problems. To illustrate this consider the following simple system on $-1 \le x \le 1$:

$$u'' = -v\,, \qquad u(-1) = u(1) = 0\,, \tag{6.15a}$$

$$\epsilon v'' + f(u')v' = 0\,, \qquad v(-1) = \alpha\,, \quad v(1) = \beta\,, \quad 0 < \alpha < \beta\,. \tag{6.15b}$$

We assume that $f(0) = 0$, $f(z) > 0$ for $z > 0$, and that $f(z) < 0$ for $z < 0$. When $f(z) = z$, this problem qualitatively resembles a subset of the drift-diffusion equations of semiconductor physics. The composite expansion for the solution to (6.15) is given in terms of an undetermined constant $c_0 > 0$ by

$$\tilde{u}^\epsilon(x) = -\frac{c_0}{2}(x^2 - 1)\,, \qquad \tilde{v}^\epsilon(x) = c_0 + \big(\alpha - c_0\big) e^{-f(c_0)\epsilon^{-1}(1+x)} + \big(\beta - c_0\big) e^{-f(-c_0)\epsilon^{-1}(1-x)}\,. \tag{6.16}$$

To determine c_0 we replace $f(u')$ in (6.15b) with $f(-c_0 x)$. Since the resulting equation is of the form given in (3.1), we can determine c_0 using the projection method. Using this method, we obtain to leading order that

$$\frac{f(-c_0)(\beta - c_0)}{f(c_0)(\alpha - c_0)} \sim \exp\left[(\epsilon c_0)^{-1}\big(F(-c_0) - F(c_0)\big)\right]\,, \tag{6.17}$$

where $F(z) \equiv \int_0^z f(\eta)\, d\eta$. Thus if $F(z) > F(-z)$ ($F(z) < F(-z)$) for all $z > 0$, then $c_0 \sim \beta$ ($c_0 \sim \alpha$) and there is no boundary layer near $x = 1$ ($x = -1$). When $f(z)$ is odd, then $c_0 = (\alpha + \beta)/2$.

We remark that if v is replaced by $-v$ in $(6.15a)$, the modified system is not exponentially ill-conditioned.

7 Exponential Small Spectral Gap Widths

We now consider three problems with exponentially small spectral gap widths.

7.1 Exponential Gap Widths and the Viscous Shock Problem

Consider $(6.1a)$ for Burgers equation ($f(u) = u^2/2$) with boundary conditions

$$u(0,t) = \alpha - A_l e^{-\epsilon^{-1} c_l}\,, \qquad u(1,t) = -\alpha + A_r e^{-\epsilon^{-1} c_r}\,. \tag{7.1}$$

Here $c_l > 0$, $c_r > 0$ and $\alpha > 0$. The slow internal layer motion for this problem was studied in [28] and [19]. Applying the Cole-Hopf transformation $u = -2\epsilon v_x/v$ to $(6.1a)$, (7.1), and separating variables by writing $v = e^{\lambda t}\phi(y)$, we obtain the eigenvalue problem

$$\begin{gathered} \epsilon\,\phi^{''} - \lambda\phi = 0\,, \qquad 0 \le y \le 1\,, \\ \phi^{'}(0) = \frac{1}{2\epsilon}\left(-\alpha + A_l e^{-\epsilon^{-1} c_l}\right)\phi(0)\,, \qquad \phi^{'}(1) = \frac{1}{2\epsilon}\left(\alpha - A_r e^{-\epsilon^{-1} c_r}\right)\phi(1)\,. \end{gathered} \tag{7.2}$$

The first two eigenfunctions are $\phi_0 = \cosh[\mu_0(x - x_0)]$ and $\phi_1 = \sinh[\mu_1(x - x_1)]$, where $\mu_0 = (\lambda_0/\epsilon)^{1/2}$, $\mu_1 = (\lambda_1/\epsilon)^{1/2}$, x_0 and x_1 satisfy some explicit transcendental equations. By analyzing these equations, we obtain the following estimate as $\epsilon \to 0$ for the exponentially small gap width:

$$\Delta\lambda \equiv \lambda_0 - \lambda_1 \sim 2\alpha^2\epsilon^{-1}e^{-\epsilon^{-1}\alpha/2}\left[1 + \frac{B^2}{16\alpha^2}\right]^{1/2}\,, \qquad B \equiv A_l e^{-\epsilon^{-1}(c_l - \alpha/2)} - A_r e^{-\epsilon^{-1}(c_r - \alpha/2)}\,. \tag{7.3}$$

The metastable time scale for internal layer motion near equilibrium is given by $\left(\Delta\lambda\right)^{-1}$. When $B = 0$, (7.3) was given in [27]. In Tables 9a, 9b we compare (7.3) with the corresponding numerical results for $\Delta\lambda$ computed using the eigenvalue solver of [21]. From these tables we observe that (7.3) determines $\Delta\lambda$ very closely and that the numerical method is able to calculate $\Delta\lambda$ even when $\Delta\lambda \approx 10^{-12}$.

7.2 Tunneling Through a High Barrier Square Well

The following exactly solveable tunnelling problem was studied in [12]:

$$\psi^{''}(x) + [\lambda - V_\epsilon(x)]\,\psi(x) = 0\,, \qquad V_\epsilon(x) = \begin{cases} \epsilon & 0 \le x < 1\,, \\ F\epsilon^{-2} & 1 < x < \epsilon^{-1} - 1\,, \\ \epsilon & \epsilon^{-1} - 1 < x \le \epsilon^{-1}\,, \end{cases} \tag{7.4}$$

with $\psi(0) = \psi(\epsilon^{-1}) = 0$. Here F is a positive constant. Let $\lambda_0(\epsilon)$ and $\lambda_1(\epsilon)$ be the first and second eigenvalues of (7.4). Then, as was shown in [12], the gap width between λ_0 and λ_1 is exponentially small and has following estimate for $\epsilon \to 0$:

$$\Delta\lambda \equiv \lambda_1 - \lambda_0 = 4\left(G_\lambda[\lambda_0(\epsilon), \epsilon]\right)^{-1}\,\exp\left[-\left(F\epsilon^{-2} - \lambda_0(\epsilon)\right)^{1/2}\left(\epsilon^{-1} - 2\right)\right]\,. \tag{7.5a}$$

Here $G(\lambda, \epsilon)$ is defined by

$$G(\lambda, \epsilon) = 1 + \tan[(\lambda - \epsilon)^{1/2}](\lambda - \epsilon)^{-1/2}(F\epsilon^{-2} - \lambda)^{1/2}\,, \tag{7.5b}$$

and $\lambda_0(\epsilon)$ satisfies the transcendental equation $G[\lambda_0(\epsilon), \epsilon] = 0$, which can be solved numerically.

When $F = 1$, in Table 9c we compare (7.5a) with corresponding numerical results for $\Delta\lambda$ computed using the eigenvalue solver of [21]. These comparisons show that, even in the presence of a strong discontinuity in the potential, the eigenvalue solver accurately computes the gap width. We remark that for the values of ϵ given in Table 9c, the limiting form $\Delta\lambda \sim 8\pi^2 \epsilon F^{-1/2} \exp\left[-F^{1/2}\epsilon^{-1}(\epsilon^{-1} - 2)\right]$, which can be obtained from (7.5a), agrees rather poorly with the numerical results.

7.3 The Forced Burgers Equation and the Double-Well Potential

Exponential eigenvalue degeneracy also occurs for the quantum anharmonic oscillator problem

$$\psi''(x) + [\lambda - V_\epsilon(x)]\,\psi(x) = 0\,, \qquad -\infty < x < \infty\,, \qquad V_\epsilon(x) = x^2(1-\epsilon x)^2\,, \tag{7.6}$$

with $\psi(x) \to 0$ as $|x| \to \infty$. The potential $V_\epsilon(x)$, has a symmetric double-well structure with wells of equal depth located at $x = 0$ and $x = \epsilon^{-1}$. Let $\lambda_0(\epsilon)$ and $\lambda_1(\epsilon)$ be the first and second eigenvalues of (7.6), respectively. An asymptotic formula for the exponentially small gap width $\Delta\lambda = \lambda_0 - \lambda_1$ was proven in [12].

We now show that an eigenvalue problem, closely related to (7.6), is relevant to describing metastable internal layer motion for the following forced Burgers equation in the limit $\epsilon \to 0$:

$$u_t + uu_y = \epsilon u_{yy} + \epsilon^{-2} f(y)\,, \qquad 0 \le y \le 1\,, \quad t > 0\,, \tag{7.7a}$$

$$u(0,t) = 0\,, \qquad u(1,t) = 0\,. \tag{7.7b}$$

Here $f(y)$ satisfies

$$f(0) = f(1/2) = f(1) = 0\,, \quad f(y) = -f(1-y)\,, \quad f'(0) > 0\,, \quad f(y) > 0 \;\text{ for }\; 0 < y < 1/2\,, \tag{7.8}$$

so that $\int_0^1 f(y)\,dy = 0$. Replacing $\epsilon^{-2} f(y)$ by $f(y)$ in (7.7), the numerical study of [18] showed that metastable internal layer motion, similar to that for (6.1), occurs for this problem. We now calculate the metastable time scale for this motion.

Setting $u(y,t) = -2\epsilon v_y(y,t)/v(y,t)$ and $v(y,t) = e^{-\lambda \epsilon^{-1} t}\phi(y)$ in (7.7), we obtain the following eigenvalue problem on $0 < y < 1$:

$$\epsilon^2 \phi'' + \left[\lambda - \epsilon^{-2} F(y)\right]\phi = 0\,, \qquad \phi'(0) = \phi'(1) = 0\,; \qquad F(y) \equiv \frac{1}{2}\int_0^y f(\eta)\,d\eta\,. \tag{7.9}$$

Then, the solution to (7.7) is recovered from

$$u(y,t) = -2\epsilon \frac{v_y(y,t)}{v(y,t)}\,, \quad \text{where} \quad v(y,t) = \sum_{j=0}^{\infty} c_j e^{-\lambda_j \epsilon^{-1} t}\phi_j(y)\,, \quad c_j \equiv \int_0^1 v(y,0)\phi_j(y)dy\,. \tag{7.10}$$

Here λ_j and ϕ_j, for $j \ge 0$, are the eigenvalues and the normalized eigenfunctions of (7.9). For (7.9) it can be shown that $\lambda_1 - \lambda_0$ is exponentially small and that $\lambda_1 - \lambda_0 = o(\lambda_2 - \lambda_1)$ as $\epsilon \to 0$. Thus, for $t \gg 1$, $u(y,t)$ can be calculated asymptotically using the first two modes in (7.10). With this approximation, we find that the slow motion shock layer trajectory $y = y_0(t)$, defined by $u[y_0(t), t] = 0$, satisfies the transcendental equation

$$\frac{\phi_0'[y_0(t)]}{\phi_1'[y_0(t)]} \sim -\frac{c_1}{c_0} \exp\left[-t/t_c\right], \qquad t_c \equiv \epsilon\,(\lambda_1 - \lambda_0)^{-1}. \tag{7.11}$$

Here ϕ_0, ϕ_1, c_0, c_1 and $\lambda_1 - \lambda_0$ all depend on ϵ. Thus, the exponentially long time scale t_c is determined by the gap width $\Delta\lambda = \lambda_1 - \lambda_0$. Since $t_c > 0$ and $\phi_0'(1/2) = 0$, it is clear that $y_0(t) \to 1/2$ for $t/t_c \to \infty$.

To calculate $\lambda_1 - \lambda_0$, we let $\psi(x) = \phi(\epsilon x)$ in (7.9) to obtain

$$\psi''(x) + [\lambda - V_\epsilon(x)]\,\psi(x) = 0\,, \qquad 0 \le x \le \epsilon^{-1}\,, \qquad V_\epsilon(x) \equiv \epsilon^{-2} F(\epsilon x)\,, \tag{7.12a}$$

$$\psi'(0) = \psi'(\epsilon^{-1}) = 0\,. \tag{7.12b}$$

From (7.8) and the definition of $F(y)$ in (7.9), it follows that $V_\epsilon(x)$ is a symmetric double-well potential satisfying $V_\epsilon(x) = V_\epsilon(1-x)$ and

$$V_\epsilon(0) = V_\epsilon'(0) = 0\,, \quad V_\epsilon''(0) = 2\beta\,, \qquad V_\epsilon[(2\epsilon)^{-1}] = \epsilon^{-2} V^* = \max_{1 \le x \le \epsilon^{-1}} V_\epsilon(x) > 0\,. \tag{7.12c}$$

Here V^* and β are related to $f(y)$ by $V^* = \frac{1}{2}\int_0^{1/2} f(y)\,dy$ and $\beta = f'(0)/4$. The main difference between (7.6) and (7.12) is that (7.12) is defined on a finite interval with no-flux boundary conditions imposed at the location of the minima of the potential. The gap width $\Delta\lambda$ for (7.12) can be calculated asymptotically by formally extending the analysis of [12] to treat an arbitrary symmetric double well potential with boundary conditions (7.12b). This analysis, for $\epsilon \to 0$, yields

$$\Delta\lambda \equiv \lambda_1 - \lambda_0 \sim \frac{4}{\sqrt{\pi}}\,\beta^{1/2} e^{-1/2}\, \exp\left(-2\int_{x_1(\epsilon)}^{(2\epsilon)^{-1}} \left[V_\epsilon(x) - \beta^{1/2}\right]^{1/2} dx\right). \tag{7.13}$$

Here $x_1(\epsilon)$ is the root of $V_\epsilon(x) = \beta^{1/2}$ for which $x_1(\epsilon) \to \beta^{-1/4}$ as $\epsilon \to 0$. Substituting (7.13) into (7.11) we obtain the exponentially long time scale t_c.

As an example, let $f(y) = \sin(2\pi y)/2$. Then, the gap width satisfies (7.13), where

$$\beta = \frac{\pi}{4}\,, \qquad V_\epsilon(x) = \frac{1}{8\pi\epsilon^2}\left[1 - \cos(2\pi\epsilon x)\right]. \tag{7.14}$$

In Table 9d we compare (7.13), (7.14) with the corresponding numerical results for $\Delta\lambda$ computed using the eigenvalue solver of [21]. For this range of ϵ, the asymptotic result provides only a moderately good determination of the gap width. We note that our computations for the numerical gap width are limited to those values of ϵ for which $\Delta\lambda$ is greater than $\Delta\lambda \approx O(10^{-13})$. Thus, we can not verify (7.13), (7.14) numerically at very small values of ϵ. The pre-exponential factor in (7.13) represents the first term in an asymptotic expansion in powers of ϵ of a more complicated, ϵ dependent, pre-exponential factor. In analogy with the example in §7.2, it is our belief that if we were able to calculate higher order corrections for this pre-exponential factor, the resulting asymptotic gap width formula would agree more closely with the corresponding numerical result, at finite ϵ, than does (7.13).

Acknowledgements

J. Y. L. would like to thank Prof. L. Greengard for helpful discussions on the numerical computations. M. J. W. is grateful to Prof. U. Ascher for introducing us to the shape from shading problem and to Prof. J. B. Keller for a helpful correspondence on the double-well problem.

References

[1] R. Ackerberg, R. E. O'Malley, *Boundary Layer Problems Exhibiting Resonance*, Studies in Appl. Math. 49, (1970), pp. 277-295.

[2] P. B. Bailey, M. K. Gordon, L. F. Shampine, *Automatic Solution of the Sturm-Liouville Problem*, ACM Trans. on Math. Software 4, (1978), pp. 193-208.

[3] A. Bohé, *Free Layers in a Singularly Perturbed Boundary Value Problem*, SIAM J. Math. Anal. 21, (1990), pp. 1264-1280.

[4] P. Carter, *Computational Methods for the Shape From Shading Problem*, Ph. D Thesis, Dept. of Comp. Sci. Univ. of British Columbia Technical Report 93-26, (1993).

[5] C. DeBoor, B. Swartz *Collocation Approximation to Eigenvalues of an ODE: the Principle of the thing*, Math. Comp. 35, (1980), pp. 679-694.

[6] P. P. N. De Groen, *The Nature of Resonance in a Singular Perturbation Problem of Turning Point Type*, SIAM J. Math. Anal. 11, (1980), pp. 1-22.

[7] B. Friedman, *Principles and Techniques of Applied Mathematics*, John Wiley & Sons Inc, Reprint of the (1956) book by Dover, (1990).

[8] I. Gladwell, D. K. Sayers, *Computational Techniques for Ordinary Differential Equations*, Academic Press, London, (1980), Chap. 9, 11.

[9] J. Grasman, B. J. Matkowsky, *A Variational Approach to Singularly Perturbed Boundary Value Problems for Ordinary and Partial Differential Equations with Turning Points*, SIAM J. Appl. Math. 32, (1977), pp. 588-597.

[10] L. Greengard, *Spectral Integration and Two-Point Boundary Value Problems*, SIAM J. Num. Anal. 28, (1991), pp. 1071-1080.

[11] L. Greengard, V. Rokhlin, *On the Numerical Solution of Two-Point Boundary Value Problems*, Comm. Pure and Appl. Math. 44, (1991), pp. 419-452.

[12] E. M. Harrell, *On the Rate of Asymptotic Eigenvalue Degeneracy*, Comm. Math. Physics 60, (1978), pp. 73-95.

[13] M. E. Hosea, L. F. Shampine, *Global Extrapolation Integrators for Solving Sturm-Liouville Problems by Shooting*, IMA J. Num. Anal. 13, (1993), pp. 397-411.

[14] J. Kevorkian, J. Cole, *Perturbation Methods in Applied Mathematics*, text in Applied Math. Sciences Series Vol. 34, Springer-Verlag, (1981).

[15] N. Kopell, *A Geometric Approach to Boundary Layer Problems Exhibiting Resonance*, SIAM J. Appl. Math. 37, (1979), pp. 436-458.

[16] H.-O. Kreiss, *Difference Approximations for Boundary and Eigenvalue Problems for Ordinary Differential Equations*, Math. Comp. 26, (1972), pp. 605-624.

[17] H. Kreiss, *Resonance for Singular Perturbation Problems*, SIAM J. Appl. Math. 41, (1981), pp. 331-344.

[18] G. Kreiss, H. Kreiss, *Convergence to Steady State of Solutions of Burgers Equation*, Appl. Numerical Math. 2, (1986), pp. 161-179.

[19] J. Laforgue, R. E. O'Malley, *Shock Layer Movement for Burgers Equation*, SIAM J. Appl. Math. to appear.

[20] J. Laforgue, R. E. O'Malley, *On the Motion of Viscous Shocks and the Supersensitivity of their Steady-State Limits*, Methods and Applications of Analysis, to appear.

[21] J. Y. Lee, L. Greengard, *A Fast Adaptive Numerical Method for Stiff Two-Point Boundary Value Problems*, submitted SIAM J. Sci. Stas. Comput.

[22] D. Ludwig, *Persistence of Dynamical Systems under Random Perturbations*, SIAM Rev. 17, (1975), pp. 605-640.

[23] B. J. Matkowsky, Z. Schuss, *Eigenvalues of the Fokker-Plank Operator and the Approach to Equilibrium for Diffusions in Potential Fields*, SIAM J. Appl. Math. 40, (1981), pp. 242-254.

[24] B. J. Matkowsky, *On Boundary Layer Problems Exhibiting Resonance*, SIAM Rev. 17, (1975), pp. 82-100.

[25] F. W. J. Olver, *Sufficient Conditions for Ackerberg-O'Malley Resonance*, SIAM J. Math. Anal. 9, (1978), pp. 328-355.

[26] D. Porter, D. Stirling, *Integral Equations*, Cambridge University Press, New York, (1980).

[27] L. G. Reyna, M. J. Ward, *On the Exponentially Slow Motion of a Viscous Shock*, Comm. Pure and Appl. Math. to appear.

[28] L. G. Reyna, M. J. Ward, *On Exponential Ill-Conditioning and Internal Layer Behavior*, J. Num. Func. Analysis and Optimization, to appear.

[29] L. A. Skinner, *Uniform Solutions of Boundary Value Problems Exhibiting Resonance*, SIAM J. Appl. Math. 47, (1987), pp. 225-231.

[30] R. Srinivasan, *A Variational Principle for the Ackerberg-O'Malley Resonance Problem*, Studies in Appl. Math. 79, (1988), pp. 271-289.

[31] P. Starr, V. Rokhlin, *On the Numerical Solution of Two-Point Boundary Value Problems II*, Technical Report 802, Yale University, Department of Computer Science, (1990).

[32] M. J. Ward, *Eliminating Indeterminacy in Singularly Perturbed Boundary Value Problems with Translation Invariant Potentials*, Studies in Appl. Math. 87, (1992), pp. 95-134.

[33] D. S. Watkins, *Some Perspectives on the Eigenvalue Problem*, SIAM Review, 35, No. 3, (1993), pp. 430-471.

[34] M. Williams, *Another Look at Ackerberg-O'Malley Resonance*, SIAM J. Appl. Math. 41, (1981), pp. 288-293.

[35] M. Williams, *Asymptotic Exit Time Distributions*, SIAM J. Appl. Math. 42, (1982), pp. 149-154.

$1/\epsilon$	λ_0 (num.)	λ_0 (3.12a) 2 term	λ_0 (3.12a) 1 term
1.0	$-2.8154935188744 \times 10^{-1}$	-2.7945×10^{-1}	-2.8846×10^{-1}
3.0	$-1.6457072776 \times 10^{-4}$	-1.6586×10^{-4}	-1.6761×10^{-4}
5.0	-7.193970×10^{-8}	-7.2134×10^{-8}	-7.2588×10^{-8}
7.0	-2.86443×10^{-11}	-2.8683×10^{-11}	-2.8812×10^{-10}
8.0	-5.6135×10^{-13}	-5.6194×10^{-13}	-5.6415×10^{-12}
9.0	-1.086×10^{-14}	-1.0921×10^{-14}	-1.0959×10^{-13}
9.5	-1.53×10^{-15}	-1.5188×10^{-15}	-1.5238×10^{-14}
10.0	-2.2×10^{-16}	-2.1093×10^{-16}	-2.1159×10^{-16}

Table 1a: Comparison of asymptotic and numerical values for λ_0 of (3.2) with $p(x) = 2\pi x^{-1}\sin(\pi x/2)$, $m = 0$, and $a = b = 1$.

$1/\epsilon$	λ_0 (num.)	λ_0 (3.12b) 2 term	λ_0 (3.12b) 1 term
12.0	$-6.1848298938 \times 10^{-5}$	-6.5684×10^{-5}	-6.8344×10^{-5}
20.0	$-3.2582667 \times 10^{-8}$	-3.3695×10^{-8}	-3.4743×10^{-8}
24.0	$-7.276407 \times 10^{-10}$	-7.4797×10^{-10}	-7.6914×10^{-10}
28.0	-1.60965×10^{-11}	-1.6477×10^{-11}	-1.6908×10^{-11}
32.0	-3.537×10^{-13}	-3.6096×10^{-13}	-3.6978×10^{-13}
36.0	-7.7×10^{-15}	-7.8742×10^{-15}	-8.0552×10^{-15}

Table 1b: Comparison of asymptotic and numerical values for λ_0 of (3.2) with $p(x) = 2\pi(1+x^2)^{-1}$, $m = 1$, and $a = b = 1$.

$1/\epsilon$	λ_0 (num.)	λ_0 (3.12c) 2 term	λ_0 (3.12c) 1 term
5.0	$-3.98321716946 \times 10^{-3}$	-4.0748×10^{-3}	-4.5049×10^{-2}
10.0	$-1.97255241 \times 10^{-6}$	-1.9804×10^{-6}	-2.0797×10^{-5}
12.0	-9.008550×10^{-8}	-9.0322×10^{-8}	-9.4065×10^{-7}
14.0	-4.07296×10^{-9}	-4.0805×10^{-9}	-4.2246×10^{-8}
16.0	-1.8287×10^{-10}	-1.8313×10^{-10}	-1.8876×10^{-10}
18.0	-8.169×10^{-12}	-8.1779×10^{-12}	-8.4008×10^{-12}
20.0	-3.635×10^{-13}	-3.6382×10^{-13}	-3.7272×10^{-13}
22.0	-1.61×10^{-14}	-1.6137×10^{-14}	-1.6495×10^{-14}

Table 1c: Comparison of asymptotic and numerical values for λ_0 of (3.2) with $p(x) = 2\pi$, $m = 1$, and $a = b = 1$.

$1/\epsilon$	C_0 (num.)	$C_0 - 1.5$
8.0	1.499999999999740	-2.600 $\times 10^{-13}$
15.0	1.49999999219	-7.812 $\times 10^{-9}$
19.0	1.49999891	-1.093 $\times 10^{-6}$
23.0	1.50145	1.446 $\times 10^{-3}$
25.0	1.5106	1.064 $\times 10^{-2}$
26.0	1.625	0.125

Table 2a: **Ex. 3.1**: Comparison of the numerical value for C_0 with the exact value $C_0 = 1.5$ at different ϵ. The parameter values in (3.24) are $b = 1$, $s = 0$, $\mu = 0$.

$z \equiv \epsilon^{-1}(b-1)$	C_0 (num.)	C_0 (3.25)
-4.00	1.99998234	1.99998238
-0.50	1.82036	1.82055
-0.20	1.64914	1.64870
0.00	1.50030	1.50000
0.10	1.42250	1.42328
0.50	1.17248	1.17302
1.00	1.04185	1.04019

Table 2b: **Ex. 3.1**: Comparison of the C_0 values as b is varied. In (3.24) we set $s = 0$, $\mu = 1$, and $\epsilon = 1/36$.

$1/\epsilon$	C_0 (num.)	C_0 (3.26b)
8.0	1.76707	1.76492
11.0	1.75670	1.75574
15.0	1.74945	1.74899
18.0	1.74608	1.74578
20.0	1.74432	1.74413
23.0	1.74302	1.74214

Table 2c: **Ex. 3.1**: Comparison of the C_0 values as ϵ is varied. In (3.24) we set $s = 1$, $\mu = 0$, $b = 1$, and $d = \pi/2$.

$z \equiv \epsilon^{-1}(d - \omega_1)$	C_0 (num.)	C_0 (3.26b)
-4.00	-0.22561	-0.22583
-2.25	-4.55763	-4.57322
-1.75	7.73796	7.71092
-1.00	2.42249	2.42122
0.00	1.74432	1.74413
1.00	1.58150	1.58143
2.00	1.52900	1.52896
4.00	1.50382	1.50386

Table 2d: **Ex. 3.1**: Comparison of the C_0 values as d is varied. In (3.24) we set $s = 1$, $\mu = 0$, $b = 1$, and $\epsilon = 1/20$.

$z \equiv \epsilon^{-1}(d - \omega_b)$	C_0 (num.)	C_0 (3.26a)
-4.00	-0.05636	-0.05653
-1.00	-2.44963	-2.46578
-0.85	-3.54966	-3.57891
-0.70	-5.78603	-5.85314
-0.20	10.88045	10.74001
0.00	6.02836	5.99282
0.20	4.41603	4.40038
1.00	2.65192	2.64938
4.00	2.02478	2.02471

Table 2e: **Ex. 3.1**: Comparison of the C_0 values as d is varied. In (3.24) we set $s = 1$, $\mu = 0$, $b = 3/4$, and $\epsilon = 1/36$.

$1/\epsilon$	C_0 (num.)	C_0 (3.29)
11.0	3.16129	2.83985
18.0	2.75742	2.59345
20.0	2.69740	2.55946
22.0	2.64942	2.53248
26.0	2.57865	2.49235
28.0	2.54913	2.47702

Table 3a: **Ex. 3.2**: Comparison of the C_0 values as ϵ is varied. In (3.28) we set $b = 2$ and $d = 4/3$.

$z \equiv \epsilon^{-1}(d - \omega_b)$	C_0 (num.)	C_0 (3.30)
-3.0	-0.00876	-0.00826
0.0	-0.18445	-0.18003
1.0	-0.59487	-0.57891
2.0	-3.30333	-3.13076
3.0	4.88651	5.03637
4.0	2.55533	2.57000
6.0	2.06061	2.06189

Table 3b: **Ex. 3.2**: Comparison of the C_0 values as d is varied. In (3.28) we set $b = 1$ and $\epsilon = 1/60$.

$1/\epsilon$	λ_N (num.)	λ_N (4.13) 2 term	λ_N (4.13) 1 term
15.0	-1.991931677513 $\times 10^{-2}$	-2.0510 $\times 10^{-2}$	-2.5637 $\times 10^{-2}$
25.0	-3.218742898 $\times 10^{-4}$	-3.2708 $\times 10^{-4}$	-3.7168 $\times 10^{-4}$
35.0	-3.76665870 $\times 10^{-6}$	-3.7929 $\times 10^{-6}$	-4.1485 $\times 10^{-6}$
45.0	-3.788847 $\times 10^{-8}$	-3.8034 $\times 10^{-8}$	-4.0751 $\times 10^{-8}$
55.0	-3.4992 $\times 10^{-10}$	-3.5077 $\times 10^{-10}$	-3.7101 $\times 10^{-10}$
65.0	-3.061 $\times 10^{-12}$	-3.0635 $\times 10^{-12}$	-3.2117 $\times 10^{-12}$
70.0	-2.813 $\times 10^{-13}$	-2.8201 $\times 10^{-13}$	-2.9463 $\times 10^{-13}$
75.0	-2.8 $\times 10^{-14}$	-2.5749 $\times 10^{-14}$	-2.6822 $\times 10^{-14}$

Table 4a: Comparison of asymptotic and numerical values for λ_N of the Hermite operator with $N = 1$ and $a = b = 1$.

$1/\epsilon$	λ_N (num.)	λ_N (4.13) 2 term	λ_N (4.13) 1 term
15.0	-1.0949321155467 $\times 10^{-1}$	-1.0255 $\times 10^{-1}$	-1.9228 $\times 10^{-1}$
25.0	-3.28048865792 $\times 10^{-3}$	-3.3451 $\times 10^{-3}$	-4.6460 $\times 10^{-3}$
35.0	-5.765094351 $\times 10^{-5}$	-5.8079 $\times 10^{-5}$	-7.2598 $\times 10^{-5}$
45.0	-7.7162465 $\times 10^{-7}$	-7.7426 $\times 10^{-7}$	-9.1689 $\times 10^{-7}$
55.0	-8.88700 $\times 10^{-9}$	-8.9042 $\times 10^{-9}$	-1.0203 $\times 10^{-8}$
65.0	-9.3026 $\times 10^{-11}$	-9.3140 $\times 10^{-11}$	-1.0438 $\times 10^{-10}$
70.0	-9.272 $\times 10^{-12}$	-9.2809 $\times 10^{-12}$	-1.0312 $\times 10^{-11}$
75.0	-9.10 $\times 10^{-13}$	-9.1194 $\times 10^{-13}$	-1.0058 $\times 10^{-12}$

Table 4b: Comparison of asymptotic and numerical values for λ_N of the Hermite operator with $N = 2$ and $a = b = 1$.

$z \equiv \epsilon^{-1}(b-1)$	C_0 (num.)	C_0 (4.26)
-20.0	2.999999155	2.999999165
-10.0	2.3993701	2.3993718
-4.0	2.06334	2.06339
-2.0	1.65588	1.65602
-0.5	0.85775	0.85787
0.0	0.49993	0.50000
0.5	0.14319	0.14303
1.0	-0.17670	-0.17668
3.0	-0.85139	-0.85188
10.0	-0.99989	-0.99991

Table 5a: **Ex. 4.1**: Comparison of the C_0 values as b is varied. In (4.24) we set $s = 0$ and $\epsilon = 1/60$.

$1/\epsilon$	C_0 (num.)	C_0 (4.29)
15.0	0.30022	0.30769
25.0	0.31690	0.31884
35.0	0.32244	0.32323
45.0	0.32515	0.32558
55.0	0.32677	0.32704
60.0	0.32737	0.32759

Table 5b: **Ex. 4.1**: Comparison of the C_0 values as ϵ is varied. In (4.24) we set $s = 1$, $b = 1$, and $d = 1/2$.

$1/\epsilon$	C_0 (num.)	C_0 (4.28)
30.0	0.65386	0.68677
50.0	0.72339	0.72991
70.0	0.74502	0.74783
90.0	0.75606	0.75764
100.0	0.75980	0.76105
110.0	0.76330	0.76384

Table 5c: **Ex. 4.1**: Comparison of the C_0 values as ϵ is varied. In (4.24) we set $s = 1$, $b = 3/4$, and $d = b^2/2$.

$z \equiv \epsilon^{-1}(d - 1/2)$	C_0 (num.)	C_0 (4.29)
-5.0	0.00631	0.00632
-2.0	0.10210	0.10227
-1.0	0.20542	0.20570
-0.5	0.26740	0.26770
0.0	0.32737	0.32759
0.5	0.37889	0.37901
1.0	0.41873	0.41889
2.0	0.46661	0.46675
5.0	0.49813	0.49823

Table 5d: **Ex. 4.1**: Comparison of the C_0 values as d is varied.
In (4.24) we set $s = 1$, $b = 1$, and $\epsilon = 1/60$.

$z \equiv \epsilon^{-1}(d - b^2/2)$	C_0 (num.)	C_0 (4.28)
-5.0	0.00714	0.00716
-2.0	0.13644	0.13674
-1.0	0.34091	0.34160
-0.5	5.19023	0.51999
0.0	7.59801	0.76105
0.5	1.05726	1.05875
1.0	1.38657	1.38807
2.0	1.99057	1.99173
3.0	2.37047	2.37108
5.0	2.62235	2.62242

Table 5e: **Ex. 4.1**: Comparison of the C_0 values as d is varied.
In (4.24) we set $s = 1$, $b = 3/4$, and $\epsilon = 1/100$.

$z \equiv \epsilon^{-1}(b-1)$	C_0 (num.)	C_0 (4.31)
-10.0	3.22489	3.24908
-5.0	2.50892	2.52004
-3.0	2.22446	2.23261
-1.0	1.80284	1.80833
0.0	1.53061	1.53488
0.5	1.40188	1.40567
1.0	1.29115	1.29457
3.0	1.06665	1.06953
10.0	1.02043	1.02327

Table 6a: **Ex. 4.2**: Comparison of the C_0 values as b is varied. In (4.30) we set $s = 0$ and $\epsilon = 1/60$.

$1/\epsilon$	C_0 (num.)	C_0 (4.33)
20.0	11.26078	11.72932
30.0	5.29738	5.28736
40.0	4.30928	4.32079
50.0	3.92005	3.92933
60.0	3.71039	3.71712
70.0	3.57790	3.58391

Table 6b: **Ex. 4.2**: Comparison of the C_0 values as ϵ is varied. In (4.30) we set $s = 1$, $b = 1$, and $d = 1/2$.

$z \equiv \epsilon^{-1}(d - 1/2)$	C_0 (num.)	C_0 (4.33)
-6.0	-0.00645	-0.00644
-1.0	-2.53919	-2.53073
-0.8	-4.91151	-4.88559
-0.7	-8.20719	-8.14192
-0.4	12.55606	12.67107
-0.3	7.43801	7.47417
-0.2	5.43367	5.45119
0.0	3.71039	3.71712
1.0	1.94728	1.94795
6.0	1.52765	1.52765

Table 6c: **Ex. 4.2**: Comparison of the C_0 values as d is varied. In (4.30) we set $s = 1$, $b = 1$, and $\epsilon = 1/60$.

$z \equiv \epsilon^{-1}(d - b^2/2)$	C_0 (num.)	C_0 (4.32)
-4.0	-0.01348	-0.01349
-1.0	-0.29143	-0.29169
0.0	-0.91938	-0.92033
0.5	-1.81480	-1.81707
1.0	-4.43427	-4.44246
2.0	10.90977	10.89166
2.5	6.08675	6.08333
3.0	4.79979	4.79847
4.0	3.97981	3.97948
10.0	3.62072	3.62072

Table 6d: **Ex. 4.2**: Comparison of the C_0 values as d is varied. In (4.30) we set $s = 1$, $b = 3/4$, and $\epsilon = 1/100$.

$1/\epsilon$	C_0 (num.)	C_0 (5.6)
22.0	2.60703	2.66667
30.0	2.65035	2.60870
40.0	2.60159	2.57576
50.0	2.57422	2.55814
60.0	2.55818	2.54717
75.0	2.54413	2.53676

Table 7a: **Ex. 5.1**: Comparison of the C_0 values as ϵ is varied. In (5.6) we set $b = 1$ and $d = 1/2$.

$z \equiv \epsilon^{-1}(d-1/2)$	C_0 (num.)	C_0 (5.6)
-2.0	9.15647	9.05677
-1.5	6.15388	6.09455
-1.0	4.33274	4.29787
-0.5	3.22815	3.20813
0.0	2.55818	2.54717
1.0	1.90537	1.90312
2.0	1.66521	1.66619
3.0	1.57685	1.57903
4.0	1.54435	1.54696

Table 7b: **Ex. 5.1**: Comparison of the C_0 values as d is varied. In (5.6) we set $b = 1$ and $\epsilon = 1/60$.

$z \equiv \epsilon^{-1}(d-4)$	C_0 (num.)	C_0 (5.15b)
-4.0	8.52468	8.68957
-3.0	3.13605	3.19671
-2.0	1.15369	1.17600
-1.0	0.42442	0.43263
0.0	0.15613	0.15915
0.5	9.4701×10^{-2}	9.6532×10^{-2}
1.0	5.7439×10^{-2}	5.8550×10^{-2}
2.0	2.1131×10^{-2}	2.1539×10^{-2}
3.0	7.7735×10^{-3}	7.9239×10^{-3}
4.0	2.8597×10^{-3}	2.9150×10^{-3}

Table 7c: **Ex. in §5.2**: For (5.14), (5.15b) we compare C_0 values as d is varied near $d = \gamma = 4$. In (5.14), (5.15b), $g(x) = 1$, $\nu = 0$, $\epsilon = 1/8$, and $y_0(x)$ is of type A.

$1/\epsilon$	λ_0 (num.)	λ_0 (asy.) (6.8)
10.0	-6.771209410691 $\times 10^{-2}$	-6.737946999085 $\times 10^{-2}$
20.0	-9.0801947630 $\times 10^{-4}$	-9.0799859525 $\times 10^{-4}$
30.0	-9.1770710 $\times 10^{-6}$	-9.17706962 $\times 10^{-6}$
40.0	-8.244615 $\times 10^{-8}$	-8.244615 $\times 10^{-8}$
50.0	-6.94399 $\times 10^{-10}$	-6.94397 $\times 10^{-10}$
60.0	-5.633 $\times 10^{-12}$	-5.615 $\times 10^{-12}$

Table 8a: Comparison of asymptotic and numerical values for λ_0 of (6.3) for Burgers equation with $\alpha = 1$, $\kappa_r = \kappa_l = 2.0$.

$1/\epsilon$	λ_0 (num.)	λ_0 (asy.) (6.9)
12.0	-2.9203067484 $\times 10^{-4}$	-2.9492219296 $\times 10^{-4}$
18.0	-1.09601753 $\times 10^{-6}$	-1.09655854 $\times 10^{-6}$
24.0	-3.62404 $\times 10^{-9}$	-3.62413 $\times 10^{-9}$
26.0	-5.3134 $\times 10^{-10}$	-5.3135 $\times 10^{-10}$
28.0	-7.7438 $\times 10^{-11}$	-7.7441 $\times 10^{-11}$
30.0	-1.1222 $\times 10^{-11}$	-1.1229 $\times 10^{-11}$
34.0	-2.41 $\times 10^{-13}$	-2.33 $\times 10^{-13}$

Table 8b: Comparison of asymptotic and numerical values for λ_0 of (6.3) for Burgers equation with $\alpha = 1$, $\kappa_r = \kappa_l = 1.0$.

$1/\epsilon$	λ_0 (num.)	λ_0 (asy.) (6.10)
15.0	-1.17355083586999 $\times 10^{-2}$	-1.17326912609947 $\times 10^{-2}$
35.0	-1.24288119 $\times 10^{-6}$	-1.24288117 $\times 10^{-6}$
45.0	-1.076715 $\times 10^{-8}$	-1.076717 $\times 10^{-8}$
50.0	-9.8212 $\times 10^{-10}$	-9.8203 $\times 10^{-10}$
55.0	-8.865 $\times 10^{-11}$	-8.867 $\times 10^{-11}$
60.0	-7.96 $\times 10^{-12}$	-7.94 $\times 10^{-12}$

Table 8c: Comparison of asymptotic and numerical values for λ_0 of (6.3) for Burgers equation with $\alpha = 1$, $\kappa_l = \infty$, $\kappa_r = 2.0$.

$1/\epsilon$	λ_0 (num.)	λ_0 (asy.) (6.11)
20.0	-9.697029317 $\times 10^{-5}$	-9.717580754 $\times 10^{-5}$
25.0	-4.33157634 $\times 10^{-6}$	-4.33331139 $\times 10^{-6}$
30.0	-1.8548979 $\times 10^{-7}$	-1.8550383 $\times 10^{-7}$
35.0	-7.72049 $\times 10^{-9}$	-7.72061 $\times 10^{-9}$
40.0	-3.14769 $\times 10^{-10}$	-3.14771 $\times 10^{-10}$
45.0	-1.2629 $\times 10^{-11}$	-1.2633 $\times 10^{-11}$
50.0	-4.9 $\times 10^{-13}$	-5.0 $\times 10^{-13}$

Table 8d: Comparison of asymptotic and numerical values for λ_0 of (6.3) for Burgers equation with $\alpha = 1$, $\kappa_l = \infty$, $\kappa_r = 1.0$.

$1/\epsilon$	λ_0 (num.)	λ_0 (asy.)
7.0	7.952873335 $\times 10^{-5}$	7.982675703 $\times 10^{-5}$
9.0	1.46135344 $\times 10^{-6}$	1.46207805 $\times 10^{-6}$
11.0	2.677719 $\times 10^{-8}$	2.677889 $\times 10^{-8}$
13.0	4.9043 $\times 10^{-10}$	4.9047 $\times 10^{-10}$
14.0	6.634 $\times 10^{-12}$	6.638 $\times 10^{-11}$
15.0	9.02 $\times 10^{-12}$	8.98 $\times 10^{-12}$
16.0	1.18 $\times 10^{-12}$	1.22 $\times 10^{-12}$

Table 8e: Comparison of asymptotic and numerical values for λ_0 of (6.14). The asymptotic result is $\lambda_0 \sim 96\, e^{-2\epsilon^{-1}}$.

$1/\epsilon$	$\Delta\lambda$ (num.)	$\Delta\lambda$ (asy.)
15.0	1.659387897453 $\times 10^{-2}$	1.659253110444$\times 10^{-2}$
25.0	1.8633266072 $\times 10^{-4}$	1.8633265860 $\times 10^{-4}$
35.0	1.75769941 $\times 10^{-6}$	1.75769941 $\times 10^{-6}$
45.0	1.522708 $\times 10^{-8}$	1.522708 $\times 10^{-6}$
55.0	1.253989 $\times 10^{-10}$	1.253991 $\times 10^{-10}$
65.0	9.991 $\times 10^{-13}$	9.986 $\times 10^{-13}$

Table 9a: Comparison of asymptotic and numerical values for $\Delta\lambda = \lambda_0 - \lambda_1$ of (7.2) with $\alpha = 1$, $A_l = A_r = 0$. The asymptotic result is (7.3).

$1/\epsilon$	$\Delta\lambda$ (num.)	$\Delta\lambda$ (asy.)
15.0	$1.712877958476 \times 10^{-2}$	$1.710318958498 \times 10^{-2}$
25.0	$1.9207082608 \times 10^{-4}$	$1.9206730823 \times 10^{-4}$
35.0	$1.81179541 \times 10^{-8}$	$1.81179508 \times 10^{-8}$
45.0	1.569572×10^{-8}	1.569572×10^{-6}
55.0	1.29257×10^{-10}	1.29258×10^{-10}
65.0	1.0289×10^{-12}	1.0293×10^{-12}

Table 9b: Comparison of asymptotic and numerical values for $\Delta\lambda = \lambda_0 - \lambda_1$ of (7.2) with $\alpha = A_l = 1$, $A_r = 0$, $c_l = 1/2$. The asymptotic result is (7.3).

$1/\epsilon$	$\Delta\lambda$ (num.)	$\Delta\lambda$ (asy.)
4.0	$-1.45886846337 \times 10^{-2}$	$-1.45885545566 \times 10^{-2}$
4.5	$-7.433900203 \times 10^{-4}$	$-7.433900041 \times 10^{-4}$
5.0	$-2.16014875 \times 10^{-5}$	$-2.16014875 \times 10^{-4}$
5.5	-3.646034×10^{-7}	-3.646032×10^{-7}
6.0	-3.61599×10^{-9}	-3.61596×10^{-9}
6.5	-2.14×10^{-11}	-2.12×10^{-11}

Table 9c: Comparison of asymptotic and numerical values for $\Delta\lambda = \lambda_1 - \lambda_0$ of (7.4) with $F = 1$. The asymptotic result is (7.5).

$1/\epsilon$	$\Delta\lambda$ (num.)	$\Delta\lambda$ (asy.)
8.0	$1.798097341 \times 10^{-4}$	$2.024533234 \times 10^{-4}$
9.0	9.7353845×10^{-6}	1.0695192×10^{-5}
10.0	3.613396×10^{-7}	3.901407×10^{-7}
11.0	9.2370×10^{-9}	9.8467×10^{-9}
12.0	1.631×10^{-10}	1.722×10^{-10}
13.0	1.99×10^{-12}	2.09×10^{-12}

Table 9d: Comparison of asymptotic and numerical values for $\Delta\lambda = \lambda_1 - \lambda_0$ of (7.12) with V_ϵ given in (7.14). The asymptotic result is (7.13).

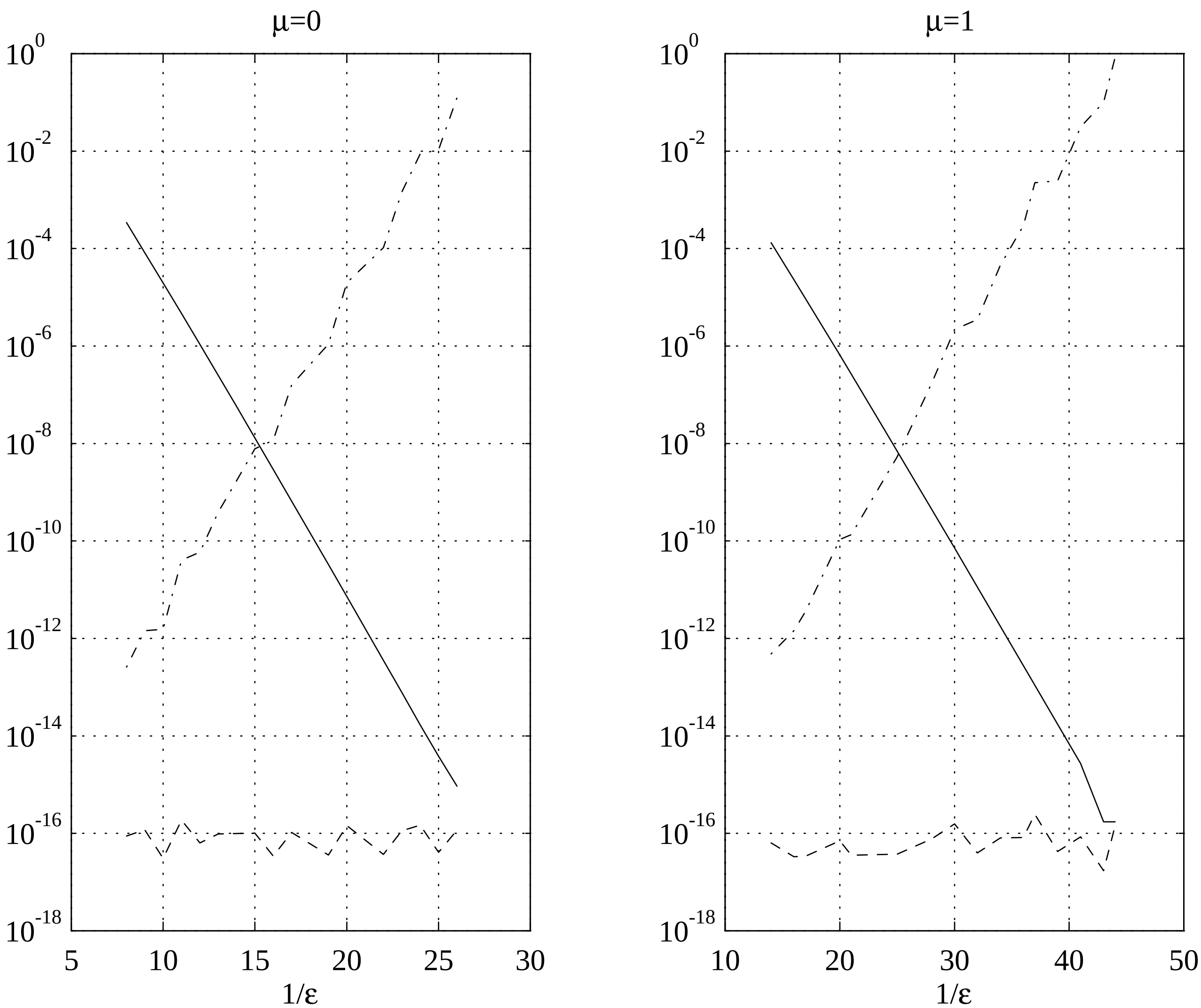

Figure 1: (Example 3.1 with $s = 0, b = 1$) The accuracy loss of C_0 as $\lambda_0 \to 0$ is plotted. The solid lines represent the computed $\lambda_0(\epsilon)$ and the dotted lines show the numerical computation error, $C_0(\epsilon) - 3/2$. The dashed lines at the bottom of the figures show the numerical error of C_0 multiplied by λ_0. Numerical values for $C_0 - 3/2$ for the case $\mu = 0$ are given in Table 2a. Numerical values for λ_0 are given in Table 1b ($\mu = 1$) and Table 1c ($\mu = 0$).

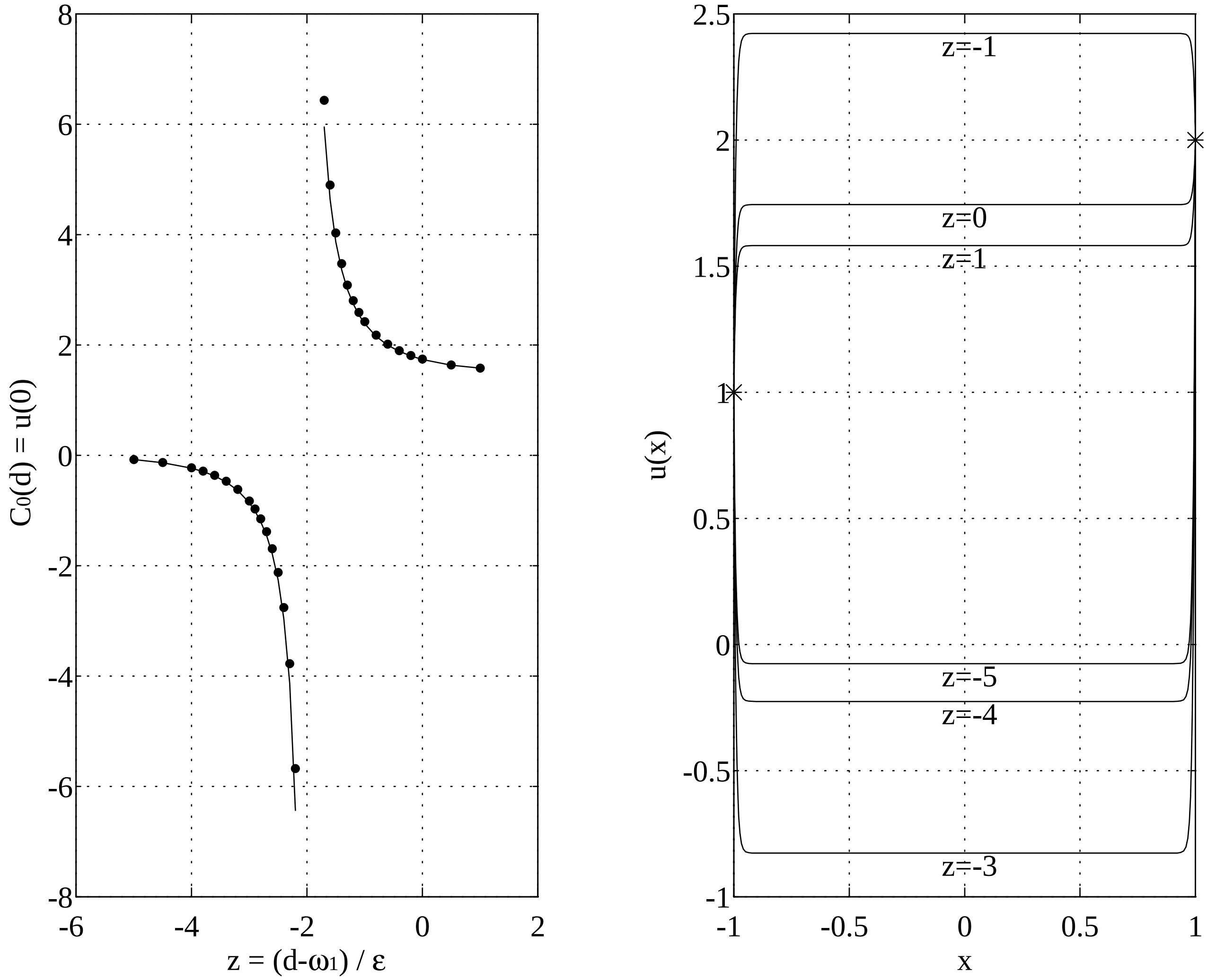

Figure 2: (Example 3.1 with $s = 1, \mu = 0, b = 1, \omega_1 = \pi/2, \epsilon = 1/20$) The solid curve in the leftmost figure shows the asymptotic result for $C_0 = C_0(d)$ obtained from (3.26b). The dotted points in this figure are the numerically computed values of $C_0(d)$ (see also Table 2d). Numerically computed solutions to (3.24) at a few selected values of d are plotted in the rightmost figure. The two $*$ marks in the rightmost figure denote the boundary data.

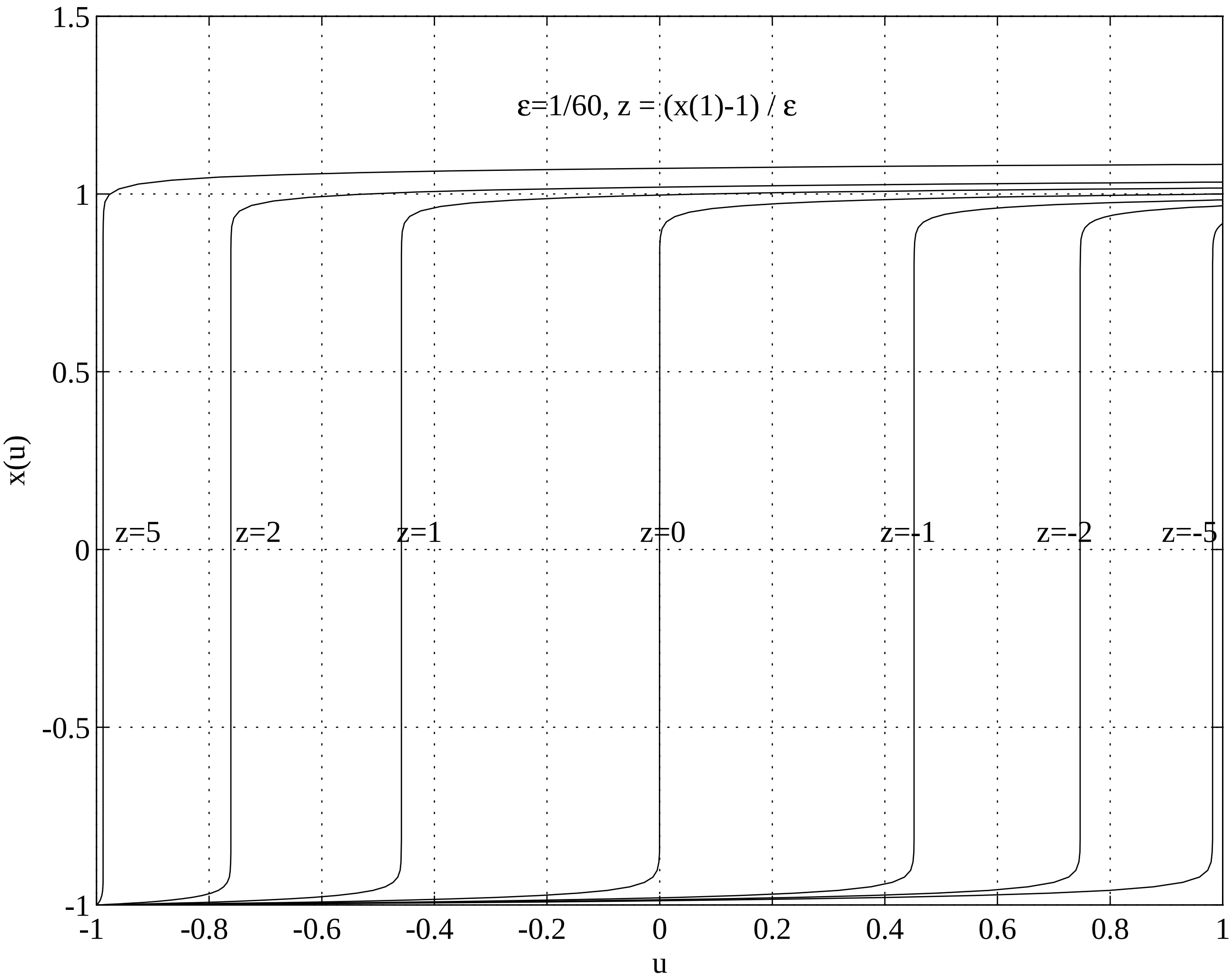

Figure 3: (Example 3.3 with $\alpha = -1, \beta = 1, \epsilon = 1/60$) The shock layer solution to (3.32) is plotted for several values of $x(1)$ for $x(1)$ near one. Notice that $O(\epsilon)$ changes in $x(1)$ causes the shock layer location to move by $O(1)$.

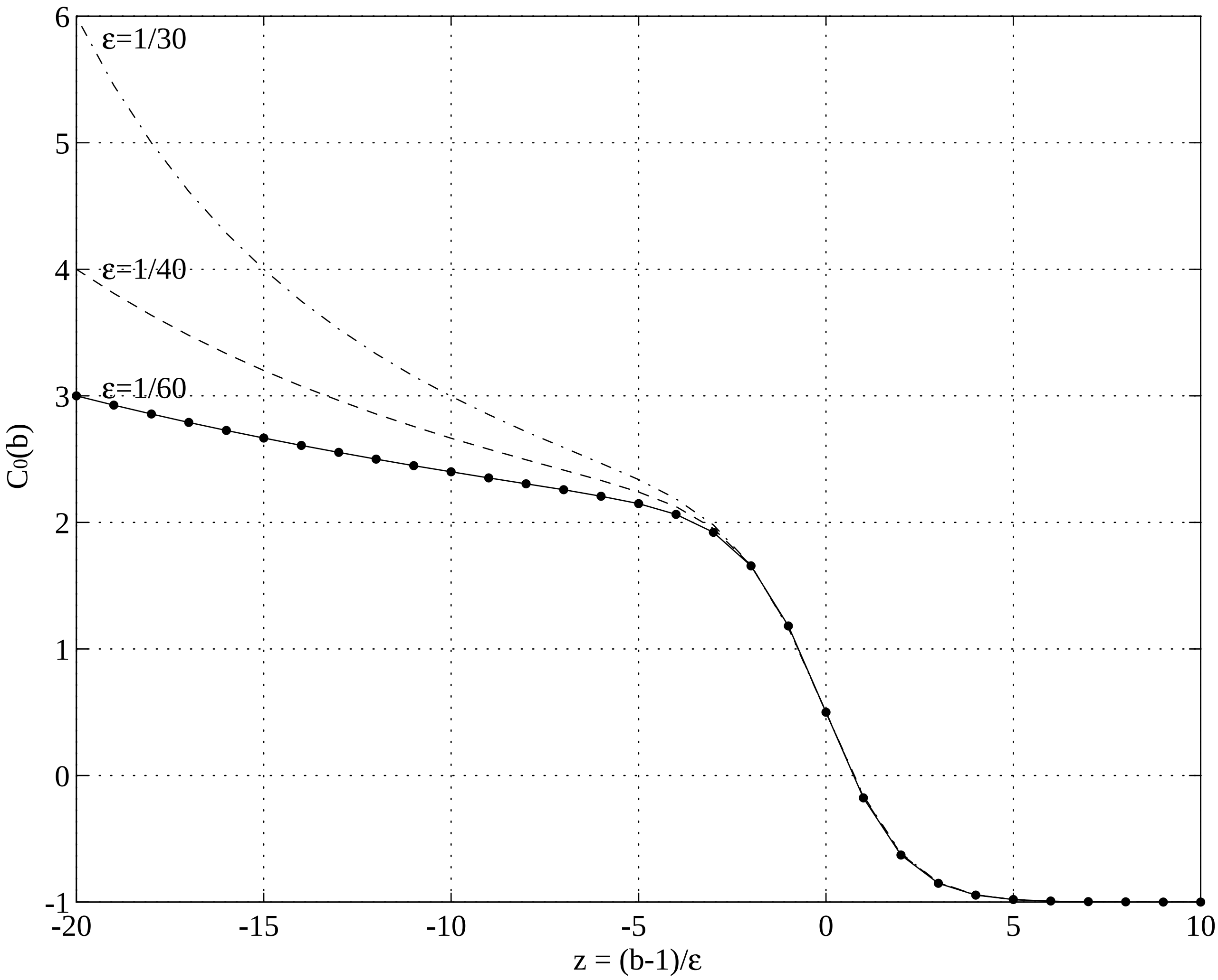

Figure 4: (Example 4.1 with $s = 0$) The solids curves show $C_0 = C_0(b)$, obtained from the asymptotic result (4.26), for three different values of ϵ. The dotted points are the numerically computed values of C_0 at a few values of b for $\epsilon = 1/60$ (see also Table 5a).

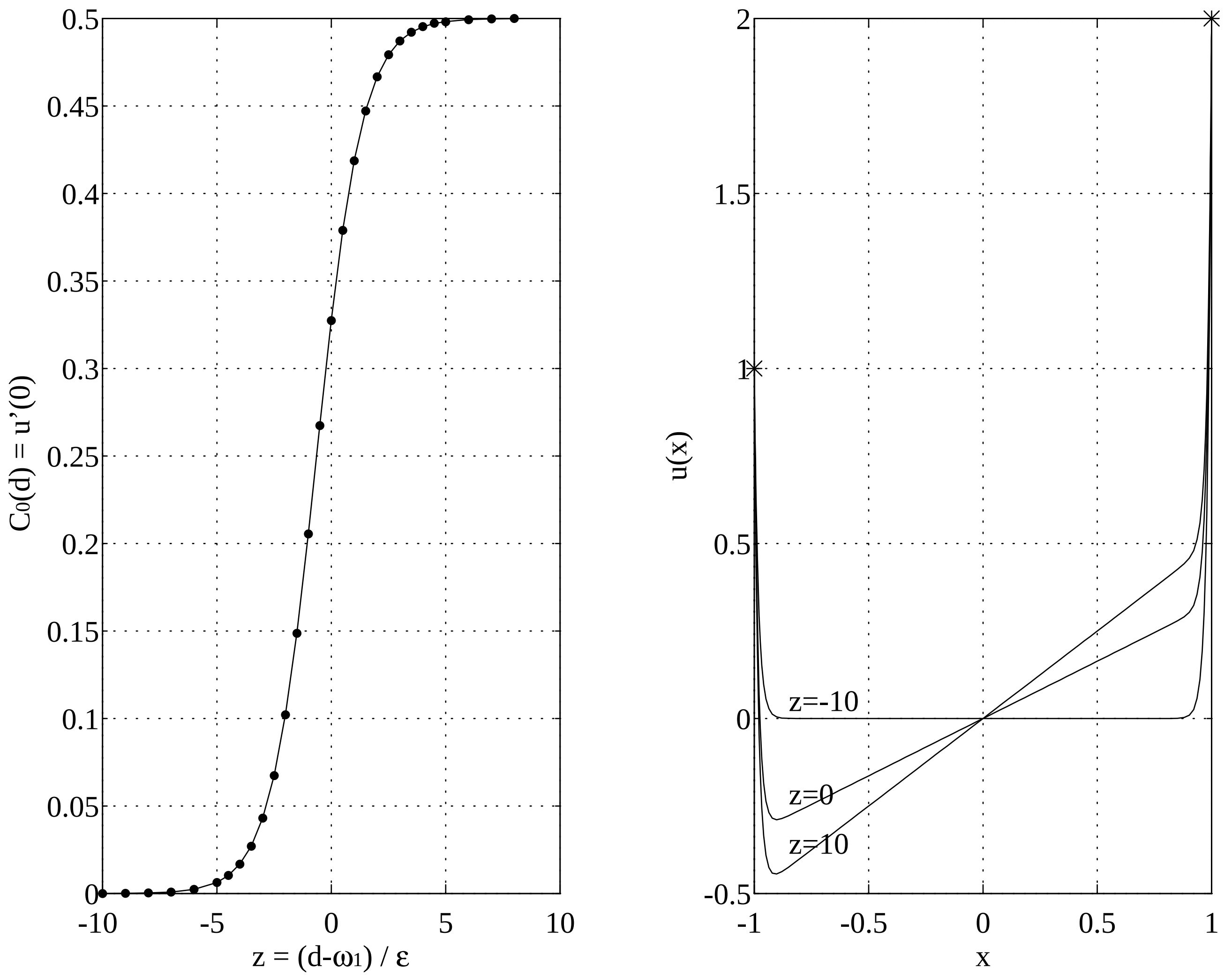

Figure 5: (Example 4.1 with $s = 1, b = 1, \omega_1 = 1/2, \epsilon = 1/60$) The solid curve in the leftmost figure shows the asymptotic result for $C_0 = C_0(d)$ obtained from (4.29). The dotted points in this figure are the numerically computed values of $C_0(d)$ (see also Table 5d). Numerically computed solutions to (4.24) at a few selected values of d are plotted in the rightmost figure. The two $*$ marks in the rightmost figure denote the boundary data.

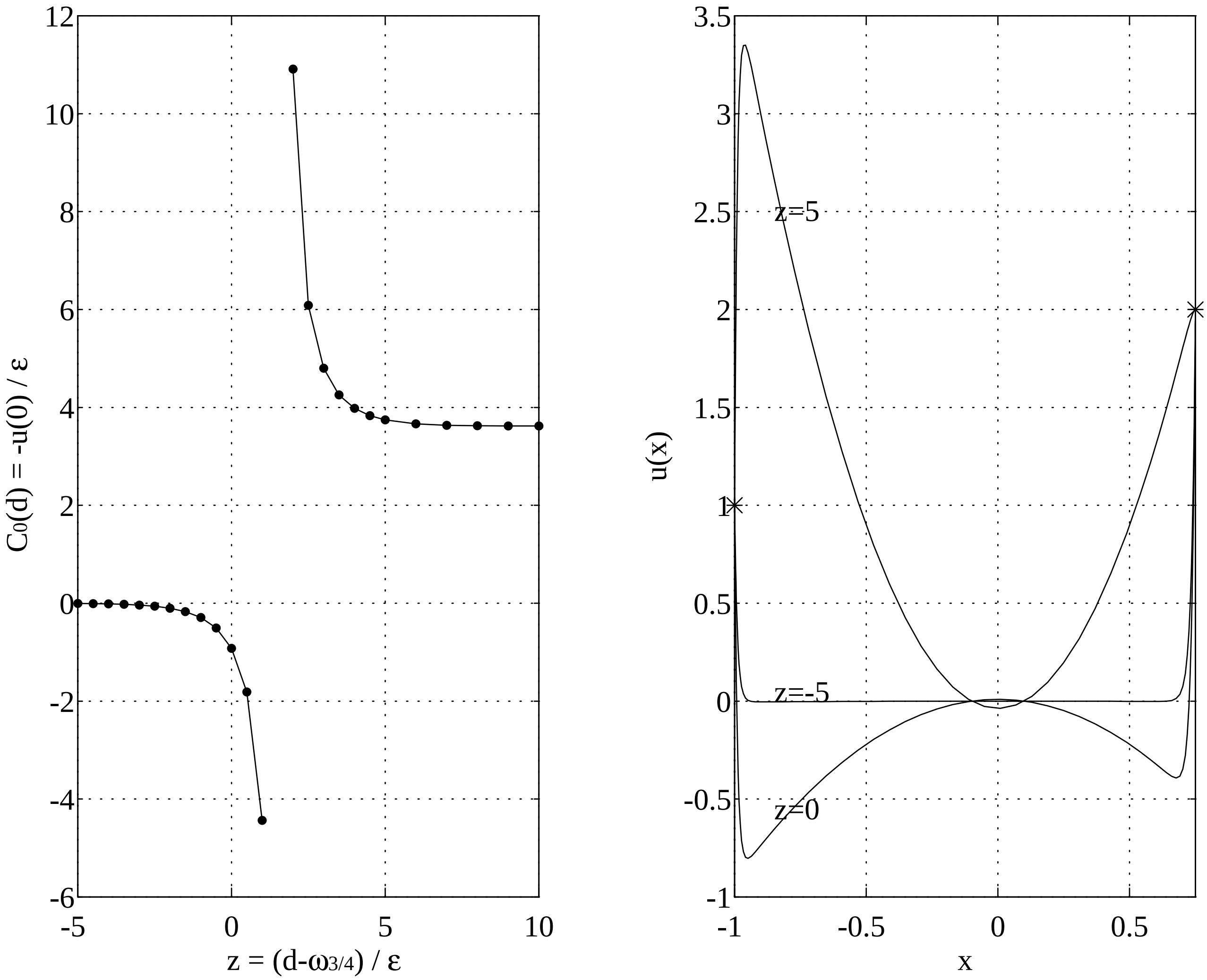

Figure 6: (Example 4.2 with $s = 1, b = 3/4, \omega_{3/4} = 9/32, \epsilon = 1/100$) The solid curve in the leftmost figure shows the asymptotic result for $C_0 = C_0(d)$ obtained from (4.32). The dotted points in this figure are the numerically computed values of $C_0(d)$ (see also Table 6d). Numerically computed solutions to (4.30) at a few selected values of d are plotted in the rightmost figure. The two $*$ marks in the rightmost figure denote the boundary data.

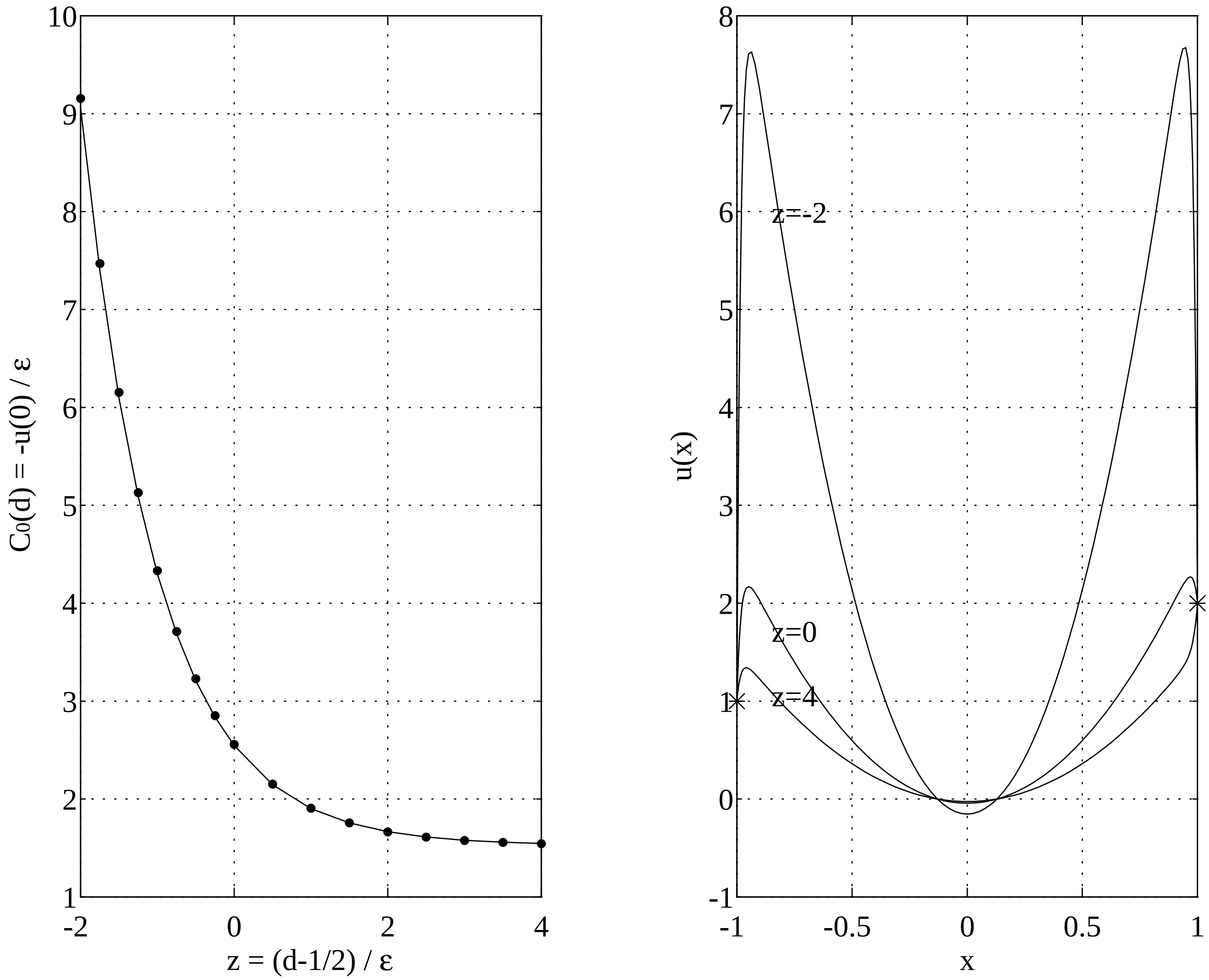

Figure 7: (Example 5.1 with $a = 1, b = 1, \nu = -5/2, \epsilon = 1/60$) The solid curve in the leftmost figure shows the asymptotic result for $C_0 = C_0(d)$ obtained from (5.6). The dotted points in this figure are the numerically computed values of $C_0(d)$ (see also Table 7b). Numerically computed solutions to (5.1) at a few selected values of d are plotted in the rightmost figure. The two $*$ marks in the rightmost figure denote the boundary data.

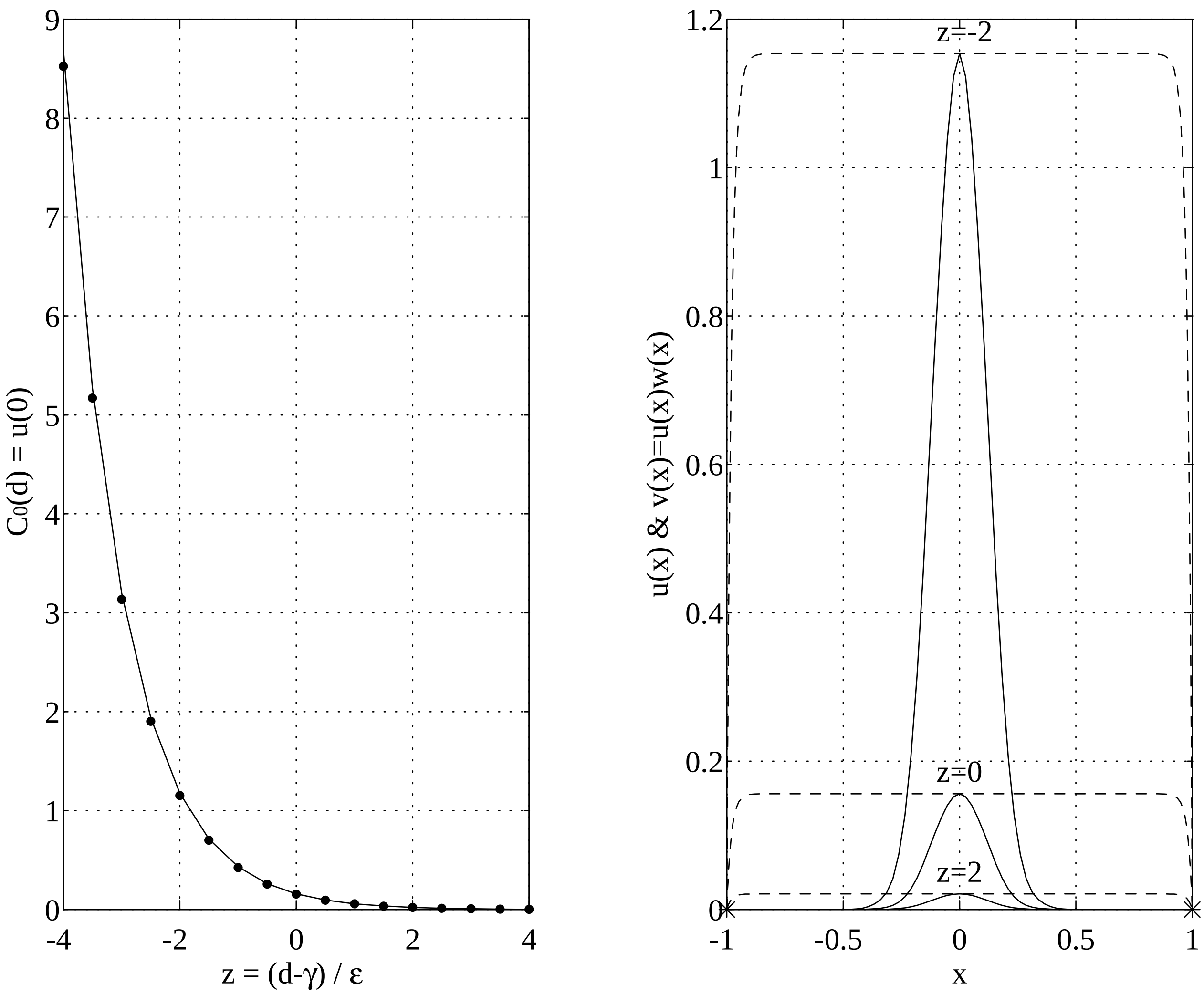

Figure 8: (Example in Section 5.2 with $\nu = 0, g(x) = 1, \epsilon = 1/8$) The solid curve in the leftmost figure shows the asymptotic result for $C_0 = C_0(d)$ obtained from (5.15b). The dotted points in this figure are the numerically computed values of $C_0(d)$ (see also Table 7c). Numerically computed solutions $u(x)$ to (5.14) (dashed curves) and $v(x) = y - y_0 = u(x)w(x)$ (solid curves) at a few selected values of d are plotted in the rightmost figure. The two $*$ marks in the rightmost figure denote the boundary data of $u(x)$.